Thermal performance of aerogel blanket thermal insulation material

by

Atiyeh Hoseini

M.Sc., Sharif University of Technology, 2013

B.Sc., Sharif University of Technology, 2011

Thesis Submitted in Partial Fulfillment of the
Requirements for the Degree of
Doctor of Philosophy

in the
School of Mechatronic Systems Engineering
Faculty of Applied Sciences

SIMON FRASER UNIVERSITY

Fall 2017

Approval

Name:	**Atiyeh Hoseini**
Degree:	**Doctor of Philosophy**
Title:	**Thermal performance of aerogel blanket thermal insulation material**
Examining Committee:	**Chair: Kevin Oldknow** Senior Lecturer
	Majid Bahrami Senior Supervisor Professor School of Mechatronic Systems Engineering
	Byron Gates Supervisor Associate Professor Department of Chemistry
	Woo Soo Kim Supervisor Associate Professor School of Mechatronic Systems Engineering
	Gary Leach Internal Examiner Associate Professor Department of Chemistry
	Ralph Evins External Examiner Assistant Professor Department of Civil Engineering University of Victoria
Date Defended/Approved:	September, 08, 2017

Abstract

The growing environmental concern throughout the world has initiated a move towards developing energy efficient technologies, which is one of the major strategies for reducing carbon emissions [1]. Increasing population has resulted in a significant increase in global energy consumption from buildings, which is ~20% to 40% in developed countries and has exceeded the industrial and transportation sectors. The rise in the time people spend inside buildings guarantees the upward trend in energy demand of both residential and commercial buildings in future [2]. In 2009, residential and commercial sectors were responsible for about 30% of total energy use in Canada, and released 28% of the associated greenhouse gas (GHG) emissions [3]. Data from 2009 suggests that 64% of household energy use and 53% of commercial energy use in Canada were for heating and cooling purposes [3]. One of the most feasible solutions for reducing the global energy consumption and associated CO_2 emissions is through usage of more efficient insulation systems in buildings [4]. As such, development of high performance thermal insulation materials is a key to save space and energy, increase comfort, and decrease environmental impact, cost, and complexity. The thermal performance of insulations is typically judged by their reported R-value (thermal resistance), determined by tests under standardized conditions, such as ASTM C177 and C518; however, designed R-value may differ from the in-service R-value for several reasons. For instance, R-value decreases when porous insulation is compressed. Temperature changes may cause some variations in thermal resistance of insulation, and all insulations are subject to absorbing moisture when they are exposed to humidity. The R-value changes are not linear, and different materials undergo different complex changes. Among available insulating material categories, *e.g.*, aerogel, foamy, fibrous, and powder, aerogels are a promising high performance type for both stationary and mobile applications.

In this research, thermal performance of aerogel blanket super insulation material will be thoroughly studied under various operating conditions, *i.e.*, temperature, compression, and humidity. A comprehensive set of accurate analytical models will be developed and verified experimentally to predict the thermal and mechanical performance of aerogel blankets. The developed concepts can be expanded to similar highly porous materials performance modelling and are applicable in thermal insulation design and selection.

Keywords: Aerogel blankets; Super insulation materials; Heat transfer; Mechanical performance; Thermal performance; Characterization

To my beloved mother, my lovely sister Leyla and the love of my life Amir Abbas

Acknowledgements

I would like to thank my senior supervisor, Dr. Majid Bahrami, for his support and guidance throughout my Ph.D. studies. It has been a privilege to work with him and learn from his experience.

I am also thankful to my supervisory committee members, Dr. Woo Soo Kim and Dr. Byron Gates, for their discussions and comments on my research project. I am also thankful to Dr. Evins and Dr. Leach for their time reading this thesis and comments. Also, I am grateful to Dr. Oldknow for being the defense committee chairman.

I would like to thank my friends and colleagues at Laboratory for Alternative Energy Conversion (LAEC) at Simon Fraser University for their support and contributions. Specially, I thank Dr. Claire McCague, LAEC's previous manager, Marius Haiducu, and LAEC's engineers, Dr. Wendell Huttema and Dr. Mehran Ahmadi, who supported this research project.

I would also like to thank the Natural Sciences and Engineering Research Council of Canada (NSERC) for the financial support through the Automotive Partnership Canada Grant.

Last but not the least; I would like to express my gratitude to my mother and my sister for their endless support and encouragement in all stages of my life. My special thanks go to my husband, Amir Abbas, for his support, and encouragement throughout my professional career. None of these would have been possible without the love and patience of my family.

Table of Contents

List of Tables

List of Figures

List of Acronyms

ASHRAE	American Society of Heating, Refrigeration, and Air Conditioning Engineers
ASTM	American Society for Testing Materials
EIA	Energy Information Administration
FTIR	Furrier Transform Infrared Spectroscopy
GHG	Greenhouse gas
HFM	Heat Flow Meter
ISO	International Organization for Standardization
MIP	Mercury Intrusion Porosimetry
RH	Relative Humidity
SEM	Scanning Electron Microscopy
TPS	Transient Plane Source
TMA	Thermo-Mechanical Analyzer

Nomenclature

A	Area (m^2)
D	Diffusion coefficient ($m^2 \cdot s^{-1}$)
e_b	Blackbody emissive power
e	Strain
m	mass
x	Volume fraction
EI	Effective flexural rigidity ($N \cdot m^2$)
F	Force (N)
k	Thermal conductivity ($W \cdot m^{-1} \cdot K^{-1}$)
K_R	Mean extinction coefficient
l	Length (m)
t	Thickness (m)
n	Index of refraction
N	Number
$\dot{q}$	Heat flux ($W \cdot m^{-2}$)
R	Resistance
r	Radius (m)
T	Temperature (K)
$T_{n\lambda}$	spectral transmittance
c	Concentration ($kg \cdot m^{-3}$)
V	Volume (m^3)
P	Pressure (Pa)

Greek Symbols

α	Deformed factor
β	Extinction coefficient
ε	Porosity
δ	Deformation (m)
λ	Wavelength (m)
σ	Stefan-Boltzmann constant
γ	Stress (Mpa)
ω	Water content
φ	Volume fraction
Λ	Mean free path

Subscripts

app	Apparent
b	Blanket
cond.	Conduction
eff	Effective
f	Fiber
g	Gas
gs	Gas solid region
m	Medium
s	Solid
tot	Total
u	Unit cell
rad.	Radiation
w	water
v	Vapor

Executive Summary

The building sector is the largest energy-consuming sector, accounting for over one-third of final global energy consumption, as well as being a significant source of carbon dioxide emissions [5]. As people spend more times in the buildings, there will be an upward trend in energy demand of both residential and commercial buildings in future [2]. By 2050, an estimated 40 exajoules (EJ) of energy, equivalent to the current energy use in Russia and India combined, could be saved in the building sector through the wide deployment of the best available technologies in the building envelope and its insulation, space heating and cooling systems, water heating, lighting, etc. [5]. Development of high-performance thermal insulation materials is a key to save space and energy, increase comfort, and decrease environmental impacts and costs. Among available insulating materials, aerogels are promising high performance materials for both stationary and mobile applications. Aerogel-based composites have the lowest thermal conductivity of any known insulation materials, providing the highest insulation properties for maximum energy efficiency accompanying less weight and thickness, and high flexibility and hydrophobicity. Aerogel-based composites also have zero Ozone Depleting Potential (ODP), which is the relative amount of degradation a chemical compound can cause to the ozone layer [6].

Aerogel, although discovered in 1960, is still not a common material and the current fundamental understanding of this material is primarily empirical. Urgent actions are needed to ensure that high-performance building envelopes rapidly gain market share and quickly become the standard for all new constructions globally. As such, aerogel blanket technology has begun receiving particular attention recently in the universal insulation market due to its prominent thermal performance [6]. This technology can address challenges posed by high-energy demands of residential and commercial buildings, where waste energy and greenhouse gas (GHG) emissions are major concerns. This research focuses on the material characterization and performance evaluation of the ultralight aerogel blanket super thermal insulation materials that provide much higher insulation property (R-values) and slower degradation over time.

Objectives

The research objectives are as follows:

- Develop an in-depth understanding of various heat transfer mechanisms involved in super thermal insulation materials and their relationship with salient micro structural parameters, such as porosity, fiber shape, size, and material.
- Characterize and study the performance of aerogel blanket super thermal insulation material in buildings. The main focus is placed on buildings envelope, however; the developed models can be used in transportation industry as well as urban farms and greenhouses to significantly reduce their energy loss, thus their environmental impacts.
- Provide a platform for predicting the thermal and mechanical performance of an enclosure, insulated using aerogel blankets under realistic conditions of temperature, humidity, and mechanical compression.

Methodology

The thesis structure and research roadmap for accomplishing the objectives is shown in Figure 1. The project is broken into two main parts; i) modeling and ii) experiments. Each part is treated separately, with different methodologies, to fill the gap in the existing literature. At the end, the results from different parts are combined and used to develop an accurate model to evaluate the thermal performance of aerogel blankets under realistic conditions.

Specifically, this research is focused on investigating: i) the effects of microstructural and morphological properties on the effective insulation value (thermal conductivity); and ii) the effects of operating conditions, i.e., temperature, relative humidity (RH), and mechanical compression on thermal properties of such porous structures. Our research utilizes advanced imaging equipment, e.g., scanning electron microscopy (SEM), Nano SEM, as well as mercury intrusion porosimetry (MIP), and Fourier transform infrared spectroscopy (FTIR) as a starting point for characterization of the micro-/nano-structure that is the key for analytical modeling of aerogel blankets.

In this study, a novel analytical heat transfer model is developed based on successful "unit-cell" approach, which is capable of relating the material properties to its micro-structure. The mathematical model accurately predicts the thermal conductivity (or R-value) of highly porous insulation materials such as aerogel blankets under operating conditions (temperature, RH, and compression). Accuracy of the analytical model is verified using the acquired data from the experimental studies.

In the experimental front, thermal, mechanical and optical measurements are conducted using commercially available samples of aerogel blankets. Two types of apparatuses for measuring thermal conductivity of porous insulation sheets are used: i) Heat Flow Meter (HFM) as per ASTM C518, ISO 8301, JIS A1412, and DIN EN 12667 standards; and ii) Transient Plane Source (TPS) as per ISO Standard 22007-2. Also, a thermomechanical analyzer (TMA) is used to measure the deformation of aerogel blankets under different mechanical loads. Additionally, to investigate the effect of moisture diffusion on thermal performance of aerogel blankets, TPS capability is improved by coupling it with a humidifier. This has been a major milestone in this research.

Contributions

The following provides an overview of the main contributions of this study:

- Developed a new geometrical model, using the concept of "unit cell", to represent the salient microstructural characteristics of aerogel blankets [1, 2].
- Developed and verified a new analytical thermal model to predict the effect of temperature on thermal performance (R-value) of aerogel blankets [1, 2].
- Developed an analytical mass transfer model to predict the water content of aerogel blankets at various temperature and humidity conditions over time [3, 4].
- Extended the analytical thermal model to humid conditions to predict the effect of moisture diffusion and temperature on thermal performance of aerogel blankets [3, 4].
- Developed and validated a new analytical mechanical model to predict the deformation of aerogel blankets under uniaxial compression [5, 6].

- Performed several experimental studies to examine the thermal performance of aerogel blankets exposed to continuous cyclic conditions of temperature, humidity, and mechanical compression [1-6].

- Combined the above-mentioned sub-models into a unified, comprehensive, and robust analytical model that is capable of accurately predicting thermal conductivity (R-value) accounting for all salient geometrical parameters, as well as operating conditions (temperature, RH, and compression) for aerogel blankets [5, 6].

References

[1] A. Hoseini, C. McCague, M. Andisheh-Tadbir, and M. Bahrami, “Aerogel blankets: From mathematical modeling to material characterization and experimental analysis,” Int. J. Heat Mass Transf., vol. 93, pp. 1124–1131, 2016.

[2] A. Hoseini, M. Andisheh-Tadbir, and M. Bahrami, “Aerogel blanket insulation: Experimental validation of analytical thermal conductivity model,” 13th SOL-GEL conference, Kyoto, Japan, September 2015 (Poster).

[3] A. Hoseini, M. Bahrami, “Effects of humidity on thermal performance of aerogel insulation blankets,” Journal of Building Engineering (Accepted).

[4] A. Hoseini, M. Bahrami, “Effect of moisture builds up on thermal conductivity of aerogel blankets,” 12th Conference on Advanced Building Skins, Bern, Switzerland, October 2017 (Oral presentation).

[5] A. Hoseini, A. Malekian, and M. Bahrami, “Experimental investigation and analytical modeling of aerogel blanket deformation and thermal performance variation under compression,” 27th International Symposium on Transport Phenomena, Honolulu, September 2016 (Oral presentation).

[6] A. Hoseini, A. Malekian, and M. Bahrami, “Deformation and thermal resistance study of aerogel blanket insulation material under uniaxial compression,” Energy and Buildings, vol. 130, pp. 228–237, 2016.

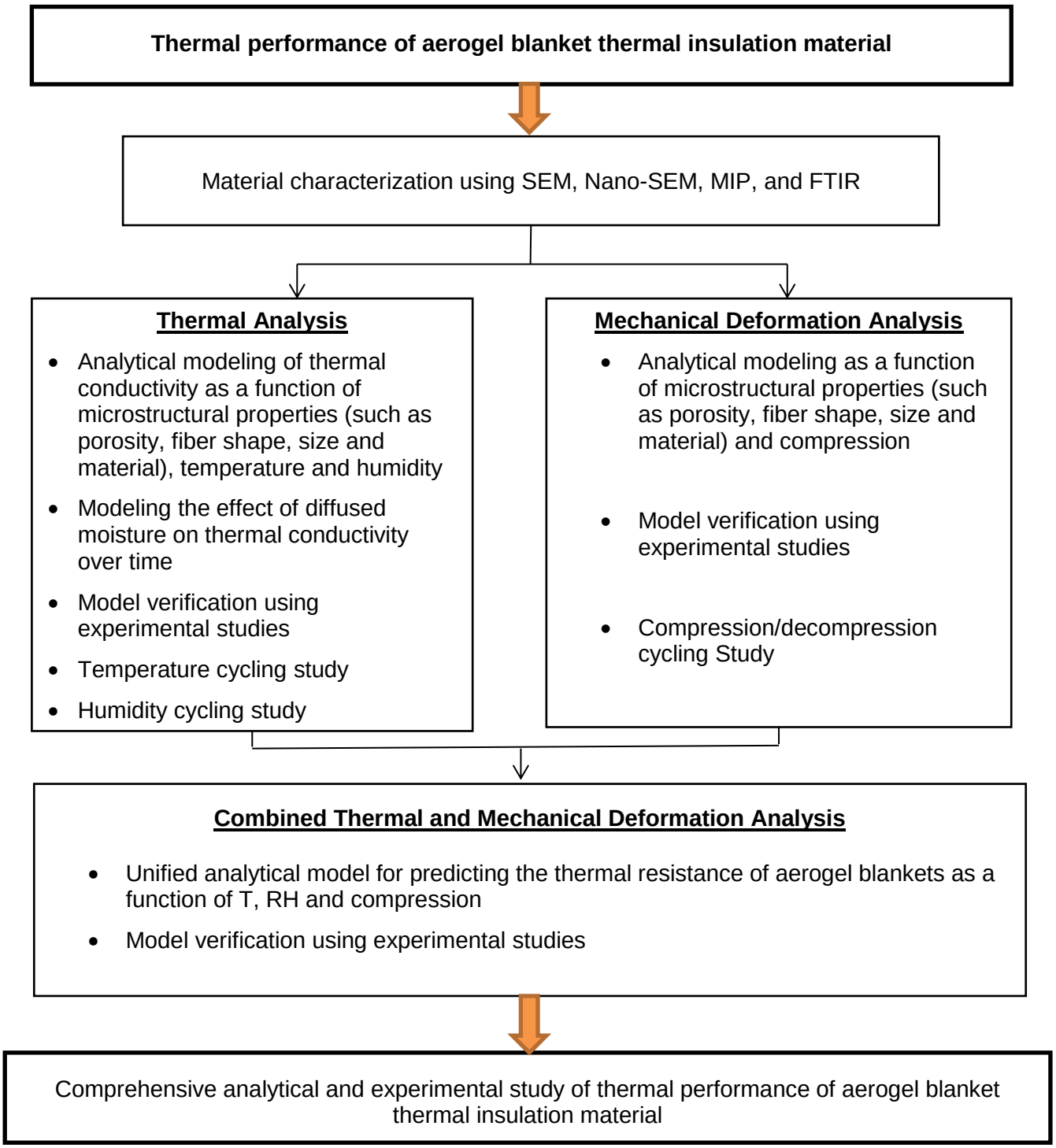

Figure 1. Scope and deliverables of the present research project.

Chapter 1.

Introduction

1.1. Research Importance and Background

As energy becomes more costly and demand grows, the use of efficient thermal insulations in buildings becomes more serious. Energy consumption in buildings accounts for 20-40% of the total energy consumption in developed countries. The growth of building energy consumption in Europe and North America is 1.5% and 1.9% per year, respectively [2]. As the U.S. Energy Information Administration (EIA) predicted in the International Energy Outlook [7], in 2030, energy consumption of houses and the non-domestic sectors will be ~67% and ~33%, respectively. By adding insulation, the amount of energy needed to heat the buildings will be lowered, which results in fewer associated greenhouse gas (GHG) emissions and a lower monthly heating expenses. The thermal performance of the building envelope remarkably depends on the thermal effectiveness of the insulation layer. Cabeza et al. [8] performed an experimental study on the energy performance of three typical insulation materials; polyurethane, polystyrene, and mineral wool. Four house-like cubicles were built and their thermal performance throughout the time was measured under the normal climatic conditions. Energy reductions up to 64% in summer and up to 37% in winter were reported. Thermal performance of building insulation is mainly determined by its k-value (thermal conductivity value) or R-value (thermal resistance value). The k-value depends on the material density, porosity, moisture content, and average temperature difference. Reported k-values by manufacturers are normally assessed at standard laboratory conditions of temperature, humidity, and mechanical load to allow a comparative evaluation of the thermal performance. However, when placed in their locations in the building envelope, thermal insulation materials are exposed to different circumstances depending on the prevailing climatic conditions, hence their actual thermal performance may extensively be different from that anticipated performance under standard laboratory conditions. This may result in major deviations in predicting the thermal and energy performance of the whole building. Abdou et al. [9] examined the variation of the k-value of seven insulation materials (*i.e.*, fiberglass, wood wool, mineral wool, rock wool, polyethylene, polyurethane, and polystyrene) under different operating temperatures. Their results showed that higher temperature leads to higher k-values and that higher insulation

density generally results in lower thermal conductivity. Bo-Ming et al. [10] measured the effective thermal conductivities of a fibrous insulation at the temperature range of 300 to 973K and claimed that effective thermal conductivity increases non-linearly with increasing average temperature of the sample. They also developed a 1-D finite volume numerical model combined radiation and conduction heat transfer to predict the behavior of the effective thermal conductivity of the fibrous insulation at various temperatures and pressures. However, in the mentioned studies the impact of accumulation of moisture within the investigated insulations and the subsequent reduction of the insulation thermal resistance, which is another major factor affecting the k-value of insulation materials, was not considered. The ambient air humidity and indoor conditions, as well as the wall or roof system moisture characteristics, play an important role in determining the moisture status of the insulation material. In hot–humid climates, condensation can happen within the insulation material, raising its moisture content. This leads to higher thermal conductivity due to the enhanced heat transfer by conduction and, under certain conditions, by the evaporation–condensation process, in which moisture moves from warm to cold regions. The presence of moisture in insulation may also contribute to corrosion and degradation under the insulation layer. Additionally, moisture buildup can result in the growth of fungus and mold, which can affect the structural reliability of building components and occupants' health [9-11]. Fan and Wen [14] and Fan et al. [15] studied the initial water content and thickness of the fibrous insulation together with the environmental temperature as the three most important factors influencing the heat flux. Björk and Enochsson [16] studied the moisture dependent heat transfer for three different thermal insulation materials: glass wool, melamine foam, and corrugated sheets of cellulose plastic. The materials were quite different with respect to condense formation and maximal moisture accumulation at similar environmental conditions. They also showed considerable differences in moisture influence on the heat transfer. Their results showed that the higher the moisture accumulation, the greater the influence of the moisture on thermal transmissivity at a steady-state condition.

Thermal insulations can be categorized in different ways [17] , based on their:

a) Structure : porous(foam), fibrous, and granulated;

b) Shape of product: loose (back fill, wool) and flat (board, mat, felt);

c) Binder content: containing binder and binder-free;

d) Type of ground substance: inorganic and organic; and

e) Reaction to fire (Euroclass): non-combustible (class A1), limited combustibility (class A2, B), combustible (class C, D, E, F).

Insulation products can also be classified according to the nature of their material [18]:

a) Light silicate substances, *e.g.*, light aggregate, light concrete;

b) Foam inorganic substances, *e.g.*, foam glass;

c) Foam organic substances, *e.g.*, foam plastics;

d) Fibrous substances, *e.g.*, glass wool and mineral (stone) wool; and

e) Organic substances, *e.g.*, cork, timber wool, and paper.

Each type of insulation material has advantages and disadvantages, in terms of durability, material stability, resistance to fire, and impact on environment and human health. Therefore, type of the building and condition specify the choice of the right insulation. Aerogel-based composite materials are also a member of building insulation materials that protects buildings and constructions against changes of the ambient and are recently being investigated due to their enhanced thermal properties. By using aerogel-based composite materials, thinner wall can be built having the same insulation R-value compared to conventional insulation materials. This characteristic is useful in big cities where space allocation is limited for new constructions and also represents an economic benefit for the owner.

Aerogels were invented in 1930 by Dr. Samuel Stephens Kistler; however, their first commercialization did not happen until 1950s [19]. Silica aerogels are the most common type of aerogels and also the ones utilized in building applications. Aerogels are prepared through a supercritical drying process that creates a highly porous open cell solid material, which feature thermal conductivities as low as 0.013 $W \cdot m^{-1} \cdot K^{-1}$ [20]. Their remarkable properties include extremely low thermal conductivity, high resistance to acoustic waves, and low dielectric constant. Aerogels function as thermal super insulators mainly by minimizing heat conduction through their low density and tortuous solid nanostructure; heat convection through very small pore sizes; and radiation by adding infrared (IR) absorbing or scattering agents in the aerogel matrix. Super-insulating silica-based aerogels are low density, typically in the range of 0.08 to 0.2 gcm^{-3}, nanostructured solids with a high porosity (>95%) and typical mesopore diameters. However, aerogels have a delicate structure with low compressive strength and high

susceptibility to fracture, which make them difficult to handle. They are also prone to settling over time, especially when exposed to vibration or thermal cycling. The settling process can form voids and lead to heat leakage in the void spaces, which is a major drawback for any powder-based insulation [21]. Therefore, more durable aerogel composites, known as fiber-reinforced aerogel blankets, have been developed. These materials have applications in aerospace, military cryogenic applications, oil and gas processing industry, and construction [6]. Aerogel blankets contain aerogel particles, fibers, and optionally, a binder. In other words, in order to be of practical use as a thermal insulator, aerogels are combined with other materials to improve strength, while retaining aerogels desirable properties. Aerogel composites typically involve molding a gel around a supporting structure (*e.g.*, lofty fibrous batting, xonotlite-type calcium silicate [22]), followed by the drying process. The aerogel and supporting structure can also be combined after formation of the aerogels. The material is mechanically stable and has low thermal conductivity ranging between 0.017 to 0.04 $W \cdot m^{-1} \cdot K^{-1}$ [23]. Figure 2 shows aerogel particles in powder and bead shape, monolithic aerogel, and aerogel blanket. In this work, we will investigate the available literature on aerogel blankets. The goal is to study their thermal performance at various environmental conditions; *e.g.*, temperature, humidity, and mechanical compression, by proposing a unified mathematical modeling for these factors. Subsequent experimental analysis will be done using different equipment, such as, HFM, TPS, humidifier, TMA, SEM, and MIP. The proposed models will be introduced as a package for predicting the thermal performance of a building insulated using aerogel blankets.

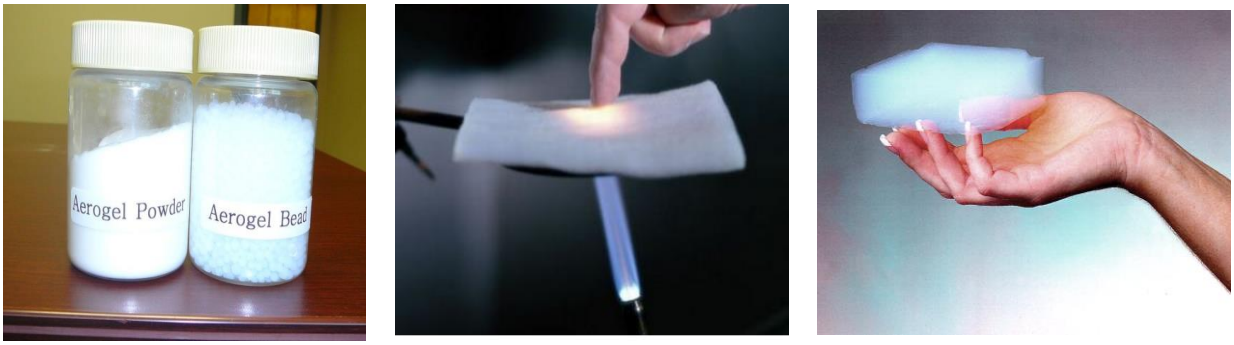

(a) (b) (c)

Figure 2. (a) Aerogel powder and beads [24], (b) aerogel blanket [25], and (c) monolithic aerogel

1.2. Relevant Literature

The parameters that contribute to the variation of the thermal insulation R-value or its thermal conductivity are documented in the ASHRAE Handbook of Fundamentals [26]. These factors emphasize on three major issues: temperature variation, mechanical abuse, and moisture penetration, which can lead to a drastic change in the expected R-value. The effect of these parameters has been long considered in building envelopes, for conventional insulation materials, as a source of a reduced quality of living and a reason of permanent damage to the building structures. Although some of these factors can be reduced by better planning and thorough monitoring, some others cannot be completely avoided and starts slow degradation and significantly decrease insulating properties of a building material. Therefore, more research is needed to be done in anticipating the thermal performance of an insulation material under various environmental conditions and also over time.

Aerogels are being investigated recently for building and transportation applications. The most common method for improving the strength of silica aerogel is adding reinforcing fibers into aerogel (it is called aerogel blanket), which also results in less conduction and radiation heat transfer. The proper fiber selection can strongly reduce the radiative heat transfer by increasing scattering and absorption [27], [28]. Manufacturers, Aspen Aerogel Inc. and Cabot Aerogel Corporation, have reported the properties of their aerogel-based products as a function of density, pressure, and composition [23]. Kyung Wha Oh et al. [29] produced a flexible and mechanically strengthened hybrid, polyethylene terephthalate (PET)/aerogel blanket, by embedding aerogel in nonwoven fiber matrix as a sound and thermal insulation material. The PET/aerogel blanket was produced by two methods; one is direct gelation of silica on PET nonwoven and the other is dipping of PET in the dispersion of silica hydrogel. Their developed hybrid PET/aerogel showed better acoustical and thermal performances compared to monolithic aerogels. Overall, aerogel blankets thermal conductivity can be lower than air at the same pressure and their exceptional insulation characteristics are due to the small size of the large number of pores. Aerogel blankets are thin (less than 10 mm), which makes them an ideal choice for space-constrained locations. Additionally, aerogel blankets may be used from cryogenic to high temperatures (<-196°C to >800°C). Summary of the major findings of the literature review is classified in the following sections.

1.2.1. Temperature Effect

Several experimental studies have been done for evaluating heat transfer mechanisms in dry aerogel blanket insulations. A heat transfer model based on the structure of aerogel-based composites is needed to understand their characteristics at various conditions. The first effective thermal conductivity model was developed based on superposition of the solid and gas conduction and radiation thermal conductivities [30]. Convective heat transfer is negligible when the pore sizes are smaller than 1 mm [25, 28]. The second type of models uses radiation and a combined solid and gas conduction [28, 29]. The combined solid and gas thermal conductivity was developed based on a periodic structure simplified from the real material structure or an empirical combined parallel and series thermal resistance model. Wei et al. [33] investigated the effective thermal conductivity of xonotlite-aerogel composite, which was a combination of hollow spherical agglomerates interwoven with xonotlite-type calcium silicate fibers. They developed theoretical and experimental analysis on thermal conductivity of silica aerogel, xonotlite-type calcium silicate, and xonotlite-aerogel composite insulation material. They modeled one dimensional heat transfer by assuming a periodic array of hollow cubic structures with connecting bars. In this model, gas and solid conduction and radiative heat transfer were considered as the modes of heat transfer inside the composite. The model accurately predicted the thermal conductivity of a specific aerogel blanket in various pressures, temperatures, and density ranges. Their results showed that effective thermal conductivity can be lowered significantly by the composite of aerogel and xonotlite-type calcium silicate at higher temperatures. The third type of modeling was developed using numerical calculations based on the meshing of the actual structure. Although the third type is more time-consuming and cannot give analytical results, it gives more precise predictions than the other two methods. Coquard et al. [34] developed a numerical model for estimating the conductive heat transfer inside nano-structured silica using a representation of their porous structure. The model took into account the porous morphology of the material at both nano and microscopic scales. A summary of the literature on the effect of temperature on dry aerogel blanket thermal performance studies is presented in Table 1-1.

Table 1-1. Summary of literature on the effect of temperature on dry aerogel blanket thermal performance.

Author(s)	Notes
Kyung Wha Oh et al. [29]	Synthesized PET/aerogel blanket using two different methods Performed experimental study of the acoustic and thermal insulation properties of PET/aerogel blanket
Coquard et al. [34]	Performed numerical modeling of conductive heat transfer inside nano-structured silica-based materials Made several conclusions on heat transfer in nano-structures silica-based materials from the analysis of the numerical results
Wei et al. [33]	Synthesized xonotlite-aerogel composite Performed experimental study on silica aerogel, xonotlite-type calcium silicate and xonotlite–aerogel composite insulation material Developed analytical model for conduction and radiation heat transfers using unit cell approach (k-value reported of 0.028-0.10 W·m1·K-1 for 300 to 800 K) Verified for low temperature ranges
J. B. Alvey [35]	Performed experimental study on four different samples of aerogel composites Proposed an analytical model for radiation heat transfer
T. Xie et al. [37]	Performed analytical modeling of conduction and radiation heat transfers using unit cell approach for aerogel powder which was related to composites (k-value reported of 0.03-0.28 W·m-1·K-1 for 300 to 1400 K)
Zhao et al. [38]	Presented radiative property and 2-D heat transfer models to investigate the relationship between the effective thermal conductivity and morphology of fiber-loaded aerogels Used the finite volume method to calculate the effective thermal conductivity of the composite

As shown in Table 1-1, there is no compact analytical relationship, capable of predicting the effective thermal conductivity of a typical aerogel blanket material supported and verified thorough experimental studies that capture the ranges of low to high temperature conditions for different structured samples. Hence, in this research, one of the goals is developing an analytical model for predicting the thermal conductivity of aerogel blankets as a function of temperature, first in dry condition (RH=0%) and then the effect of humidity will be added to it. Material characterization has been performed to provide the input properties of the model, and experimental tests of thermal conductivity in various temperatures have been implemented for validating the model for two different commercially available samples.

1.2.2. Humidity Effect

Over the last few decades, it has been established that extensive failures in the performance of building components are often a result of thermal and moisture loads [39]. Temperature and humidity greatly affect the k-value of thermal insulations as well as indoor

conditions [26]. There are several studies that investigated the mechanism of moisture diffusion into porous materials as well as the effect of this phenomenon on variation of the k-value of conventional insulation materials. In the field of moisture diffusion analysis, Alvarez [40] experimentally studied different moisture diffusion models. He also developed an experimental apparatus to measure moisture transfer properties in porous materials under non-isothermal conditions. García et al. [38,[42] performed a set of experiments to determine the diffusion coefficient of non-impregnated transformer insulating paper and oil-impregnated transformer insulating paper as a function of temperature, moisture concentration, insulation thickness and ageing degree of the insulation paper. Stephenson [43] used a set of published results on glass fiber insulation to estimate its thermal diffusion coefficient. His hypothesis was based on that moisture diffusion is related to the gradients of temperature and concentration at the same time. He concluded that the thermal vapor diffusion coefficient is approximately five times the coefficient for the diffusion due to the gradient of the vapor density.

Several studies have been performed on thermal performance of insulations in humid conditions. Thermal conductivities of brick [44], lime-based renders [4, 5], and stone wool [47] were reported to grow quite a few times when the measured values were compared in two different states: dry and water vapor saturated conditions. The effect of moisture content on the k-value of fibrous insulations was investigated in Ref. [48] and a relationship was presented to find the thermal conductivity at various moisture content at 24°C and 34°C. They showed that higher temperatures and higher moisture content was accompanied by higher thermal conductivity in fibrous insulations, which was more pronounced in lower density materials. Jerman and Cerny [49] showed that the thermal conductivity of all mineral wools increased significantly with increasing moisture content; which was from the range of 0.10–0.14 $W \cdot m^{-1} \cdot K^{-1}$ to 0.7–0.9 $W \cdot m^{-1} \cdot K^{-1}$ at saturation. Ochs et al. [50] modified the analytical model of Krischer and Kast [51] for the effective thermal conductivity of porous materials having moisture content by adding the concept of closed pore to the humidity model. They verified the model for expanded glass granules and expanded clay using experimental data of guarded heating plate device.

Based on the above, it can be concluded that: i) moisture transport in building materials is directly responsible for structural damage; and ii) neglecting the moisture dependence of thermal conductivity of insulations, specifically aerogel-based composites, in energy-related evaluations can lead to significant errors in heat loss calculations.

Because of the outstanding insulating properties of aerogel-based composites, they drew an immense interest in recent years for many applications. Table 1-2 summarizes the studies that have been performed on aerogel-based materials at humid conditions:

Table 1-2. Summary of the available studies on aerogel and aerogel-based composites at humid conditions.

Author(s)	Notes
Lakatos [52]	Experimental study of aerogel blankets thermal-physical properties after wetting Building Energy Simulations to show the effect of moisture on heat energy demand and primary energy demand
Galliano et al. [53]	Experimental study of transient hygrothermal properties of aerogel-based and perlite composites for internal retrofit of a wall Software simulations to evaluate transient hygrothermal properties by solving coupled heat and moisture transfer
Stahl et al. [54]	Highly insulating material using aerogel granules was developed Experimental measurements of thermal conductivity and water vapor transmission resistance of the material
Ihara et al. [55]	Experimental measurements of water uptake of aerogel granules Found that the liquid water enters the nano-pores of the aerogel granulate and damages the structure and requires a long time to dry
Wakili et al. [56]	In-situ measurement of temperature, humidity, and heat flux on aerogel-based plasters Not able to reach a quasi-steady state condition in about a year Combined transient heat and moisture transfer suggested as future work

As Table 1-2 indicates, in the literature, there is a lack of systematic theoretical and experimental investigation of k-value of aerogel-based materials at humid conditions. Therefore, there is a great need for developing analytical models that can accurately predict their thermal conductivity at various climatic conditions. The goal of this research is to identify the effect of moisture diffusion on thermal performance of aerogel blankets by presenting a combined experimental and theoretical study of heat and moisture transfer.

1.2.3. Mechanical Compression Effect

The higher R-value of building insulation corresponds to its better theoretical effectiveness. In many cases, instead of changing an insulation layer, it is economically desirable to install an additional layer on top of the insulation that is already in place. Compression affects the nominal R-value of the insulators, so that the additional layer may result in a lower R-value, which is not desirable. Yarbrough et al. [57] studied the reduction of thermal resistance of loose-fill insulations due to mechanical compression and measured the thickness reduction as a function of applied load for samples of fiberglass batt, loose-fill fiberglass, loose-fill rock wool, and loose-fill cellulosic insulation. Their results showed that the

low-density materials were affected the most, showing up to 40% thickness decrease under 0.14 kPa load. Also, they showed that reduction in thermal resistance under compression was greatest for the fiberglass insulations (~20% under 0.14 kPa load). Adams and Hust [58] investigated the reduction of thermal conductivity under compression for five common porous insulation products; cellulose, rock/slag wool, bonded and un-bonded glass fiber, and a glass fiber blanket. Graves and Yarbrough [59] measured the R-values of six commercially available fiberglass batts at their full thickness and compressed to 50% of full thickness, following ASTM C518 test methods. They observed that the decrease in thermal resistance during compression was greater for samples with higher density (compression to 50% of full thickness of higher density products reduced the R-value by 45%). Symons et al. [60] studied blanket form materials, *e.g.*, low density fiberglass, sheep wool, and polyester fiber, as well as loose-fill form materials, *e.g.*, cellulose fiber, sheep wool, and rock wool, following ASTM C518 standards. Their results showed that of the materials tested, the fiberglass blankets had the lowest thermal conductivity (~0.032 $W \cdot m^{-1} \cdot K^{-1}$), requiring less thickness (~80 mm) to achieve the target thermal resistance values of 2.5 $m^2 \cdot K \cdot W^{-1}$ for a building in Australia. Kolich et al. [61] studied the thermal and physical properties of internal car insulation materials at -20 to 60ºC and 0 to 60% compression. They determined specific heat of the samples, following ASTM E1269-05, and their volume density using ASTM C302-95. They also correlated increases in apparent thermal conductivity of uniform porous materials with increasing density, and found that the apparent thermal conductivity of laminated materials (*e.g.*, foam plastic-leader) decreased with increasing density, which was caused by variation in the shape of the pores.

To the best of our knowledge, there are only a few limited studies on the relationship between thickness, compression, deformation, and thermal performance of aerogel-based composite insulation materials. A summary of available studies on aerogel composites is presented in Table 1-3.

Table 1-3. Summary of available studies on thickness or density of aerogel-based composites.

Author(s)	Notes
Erdem Cuce et al. [62]	Investigated optimum thickness of aerogel blanket insulation to maximize energy saving and thermal comfort Determined dependency of annual energy use on insulation thickness
Gupta and Ricci [36]	Fabricated aerogel/epoxy composites Studied the composites (density of 980 and 1070 $kg \cdot m^{-3}$) under compressive loads (0-120 MPa) Observed some cracks but no strength loss at 25% compressive strain
Bardy et al. [63]	Tested samples of prototype and product-line aerogel insulating blankets for thermal conductivity and compressive strain at incremental loads up to 1.2 MPa Found that the prototype sample has higher resistance under compression and recovers to its original thickness upon decompression
Duoqi Shi et al. [64]	Fabricated ceramic-fiber-reinforced SiO_2 aerogel Investigated the composite properties under compression (up to 1.5 MPa for in-plane and 16 MPa for out-of-plane compression) at high temperatures (up to 900ºC) Found that in-plane Young's modulus increases with temperature, but out-of-plane modulus decreases with temperature
Wu et al. [65]	Fabricated multilayer fiber-reinforced aerogel composites using glass fiber and SiO_2 aerogel Used unit cell approach to model the conductive heat transfer in the composite Improved the mechanical strengths of the aerogel composites via impregnating multilayer aligned fibers into aerogels Studied the effect of fiber alignments on the compressive and bending strengths and thermal conductivity of the composites

Our literature review indicates that the effect of compression on the thermal performance and structural deformation of aerogel blankets has not been thoroughly studied yet. Silica aerogel can crack and separate from the fibrous matrix, which affects the thermal resistance of the aerogel blanket insulation. As such, the focus of this research is to measure the thermal performance of two types of aerogel blanket samples under compression and after repeated mechanical load cycling. Additionally, a mechanistic analytical model is developed, following a unit cell approach, for predicting the deformation of the aerogel blankets as a function of compressive mechanical load. Bending of fibers is considered as the main deformation mechanism at the unit cell level and the overall blanket deformation is calculated from the summation of the deformations of all the layers. Employing the proposed model, a compact relationship between compressive strain and applied load (stress) is presented, which is verified using the experimental data that can be employed in predicting the deformation of any fibrous insulation material at a particular density.

1.2.4. Lack of the Literature

The previous section on literature review indicated that the focus of the pertinent research in the area of the thermal insulation materials has been mostly on conventional insulations, with some experimental studies on aerogel and aerogel-based insulation materials. There is not an in-depth study to investigate the aerogel blanket insulation material thermal performance. The present study aims to address this shortcoming by investigating the effect of realistic operating conditions, e.g., temperature, humidity, and also mechanical compression on thermal performance of aerogel blankets, in order to be used as an efficient building/greenhouse envelope. In our quest to study this material, mathematical models are developed and supported by material characterization, then verified using experimental studies. These models can be utilized in predicting the actual thermal performance of buildings and in design and development in construction industry.

Chapter 2.

Aerogel Blanket Thermal Analysis

The porous nature of aerogel blanket makes it necessary to define an effective thermal conductivity, to predict its k-value under various operating conditions and optimize its thermal performance in new designs. In general, for aerogel blankets, there are nano/meso-scale pores and matrix, as well as micro-scale additives, such as fibers and opacifier. The heat transfer modes include gas conduction, solid conduction, and thermal radiation. These multi-scale topology structures make multi-mode heat transfer to be enormously complex. The purpose of this study is to provide an analytical model for calculating thermal conductivities of silica aerogel composite insulating materials in which heat conduction and thermal radiation are taken into account simultaneously. Random and complex microstructure of the aerogel blanket is modelled following unit cell approach, which has been used for porous media by several researchers, *e.g.*, [66]–[68]. A unit cell is a small geometrical block that can describe main salient properties of the medium and is assumed to be repeated throughout the structure. Using the observations of Aspex Explorer SEM imaging, the proposed unit cell is assumed to be a 'packed bed' of spherical aerogel particles with more than 90% porosity and a solid cylindrical fiber at the center. A new analytical model for predicting the thermal conductivity of aerogel blankets as a function of temperature and relative humidity is proposed and validated for two types of aerogel blankets. Moreover, a parametric study is performed to investigate the effect of key parameters on the effective thermal conductivity of aerogel blankets, which is presented in the results and discussion section.

2.1. Mechanisms of Heat Transfer in Insulations

2.1.1. Conduction

Thermal conductivity is a measure of the amount of heat that flows through a material by conduction heat transfer. The measurements are based on Fourier's law of heat conduction:

$$\dot{q} = -k\frac{dT}{dx} \tag{1}$$

where $\dot{q}$ is heat transfer per unit area, T is the temperature, x is the direction of heat flow, and k is the thermal conductivity coefficient. Conduction occurs in solids, liquids, and gases. Gases have lower thermal conductivity than solids or liquids, therefore, for thermal insulations, where minimum heat transfer is desirable, small volume fraction of solid material and large volume fraction of gas, such as air, is required.

2.1.2. Convection

If conduction was the only pathway of heat transfer, then obviously, the best for insulation materials would be to fill large voids with low conductivity gases. However, due to the motion of gas molecules, convective heat transfer also plays an important role in thermal insulation performance. Gas particles in contact with a heat source participate in a conductive heat transfer and then move away due to buoyancy or other forces, from the original location until the next collision, where further conduction takes place. The solution to this is to break up the volume of gas pore into a large number of small voids till the contribution of convection to the overall heat transfer becomes negligible [31], [38], [69].

2.1.3. Radiation

Thermal radiation is the heat transferred through electromagnetic waves and generally is defined as following:

$$\dot{q} = \varepsilon \sigma T^4 \tag{2}$$

where ε is the emissivity and σ=5.7×10^{-8} W·m^{-2}·K^{-4} is Stefan-Boltzmann constant. The emissivity is an indication of how opaque the material is to thermal radiation. Although both conduction and convection are driven by a temperature difference, radiation is driven by a difference of the fourth power of (absolute) temperature. This means that for low temperature differences, radiation can be comparable to the other modes of heat transfer, but at higher temperature differences, radiation becomes much more dominant. For thermal insulation in building envelopes, radiative heat transfer plays a significant role. The method of calculating the radiative contribution to apparent thermal conductivity in insulating materials will be discussed in this work.

2.1.4. Effective Thermal Conductivity

Thermal insulation is designed to retard the heat flow from one region to another; the mentioned heat transfer takes place through a combination of conduction (gas and solid) and radiation. Usually, the measurement of pure conduction is challenging, therefore, measured thermal conductivities of insulating materials include all modes of heat transfer and it is called "effective" thermal conductivity. For modeling the heat transfer, thermal resistance network, which is the electric circuit analogy, is typically being used. The thermal resistances are called R-value and defined using the effective thermal conductivity as followed:

$$R = \frac{t_s}{k_{eff}} \tag{3}$$

where t_s is the material thickness.

Aerogel blankets have low thermal conductivity, due to (1) the high porosity, the small fiber-fiber contacts, and the very long solid conduction path through the aerogel skeleton, which reduce the solid thermal conduction [1,2]; (2) the restricted gas mean free path with restricted molecular collisions in the nano-pores, which reduces the gaseous thermal conduction [1,2,30]; and (3) the large extinction coefficient due to the fibers, which reduce the radiative heat transfer.

2.2. The present Model

The proposed geometrical model for the unit cell approach is shown in Figure 3. It consists of two domains: a rigid solid cylindrical fiber; and a spherical aerogel packed bed around it, both into a noticeable void space.

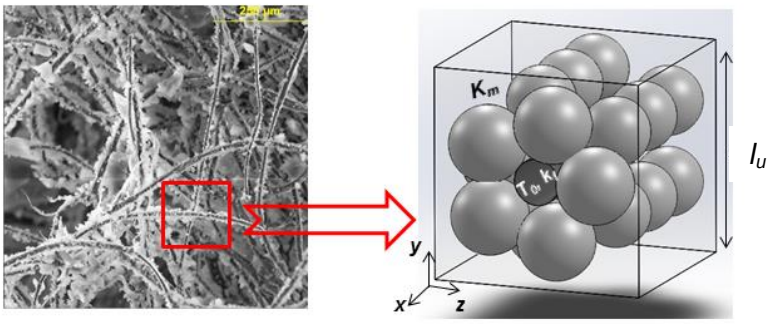

Figure 3. Proposed unit cell for aerogel blanket geometrical modeling.

The assumptions used in the model development are listed below:

- Steady-state one-dimensional heat transfer in the medium;
- Negligible natural convection due to small pore sizes (<4 mm); one can calculate the Rayleigh number based on the pore size to be Ra~10^{-10},which is significantly lower than 1708, which is the threshold for natural convection to be a considerable contributing mechanism in enclosures [33];
- Smooth spheres and fiber surfaces, *i.e.*, no roughness between contacting spheres and the fiber;
- Simplified fiber orientation and morphology to calculate the solid thermal conduction; and
- No heat generation source in the medium.

Therefore, the unit cell modeling consists of two parts: 1) Solid and gas (fluid) conduction heat transfer modeling of the cylinder and its surrounding medium, and 2) Radiation heat transfer modeling of the unit cell. Presented in Eq. (4), solid-gas conduction as well as radiation are modeled as two parallel paths of one dimensional heat transfer in aerogel blankets [70], which for both of them, coefficients are defined and modeled in the following sections:

$$\dot{q}_{tot} = k_{eff} A \frac{dT}{dz} = \dot{q}_{cond.} + \dot{q}_{rad.} \tag{4}$$

2.2.1. Conduction heat transfer

Conduction heat transfer in the unit cell is a function of the fiber and medium thermal conductivities. Following [71], a compact relationship for thermal conductivity of an infinite cylinder (fiber) in an infinite medium (aerogel packed bed) with a linear temperature gradient can be developed. The summary of the equations that lead to the final relationship for conduction heat transfer is presented below:

$$\frac{T}{T_{fiber}} = [1 - \frac{k_{fiber} - k_m}{k_{fiber} + k_m}(\frac{r_{fiber}}{r})^2]Z$$
$$Z = \frac{z}{r_{fiber}} \tag{5}$$
$$z = r\cos(\theta)$$

where k_{fiber} and k_m are thermal conductivities of the fiber and its surrounding medium, respectively and r_{fiber} is the fiber radius. l_u is the unit cell length calculated using following equation:

$$\varepsilon_b = \frac{V_{void}}{V_{tot}} = \frac{(l_u{}^2 - \pi r_{fiber}{}^2)\varepsilon_m}{l_u{}^2} \tag{6}$$

Here, V_{void} is the volume of the unit cell empty spaces, V_{tot} is the total volume of the unit cell, and ε_b and ε_m are blanket and medium porosities, respectively. In this study, blanket porosity is measured by mercury intrusion porosimetry (MIP) and the porosity of aerogel packed bed exists in the literature [72] as the medium, so that unit cell length has been calculated afterwards using Eq.(6).

Having the temperature distribution in the proposed unit cell, the effective conduction heat transfer coefficient of the blanket can be calculated using Eq.(7):

$$k_{cond.} = \frac{k_m \left.\frac{\partial T}{\partial z}\right|_{\frac{l_u}{2}}}{\frac{\Delta T\Big|_{-\frac{l_u}{2}}^{\frac{l_u}{2}}}{l_u}} \tag{7}$$

Simplifying Eq.(7) yields a compact relationship for the contribution of conduction heat transfer in the effective thermal conductivity of the blanket.

$$k_{cond.} = \frac{k_m[4\sqrt{2}(\frac{r_{fiber}}{l_u})^2(k_{fiber} - k_m) + 1.77(k_{fiber} + k_m)]}{-4\sqrt{2}(\frac{r_{fiber}}{l_u})^2(k_{fiber} - k_m) + 1.77(k_{fiber} + k_m)} \tag{8}$$

Thermal conductivity of the porous medium around the fiber containing dry air and aerogel particles

In Eq.(8), k_m is the aerogel packed bed (as the medium around the fiber) thermal conductivity, which consists of conduction of fluid inside the pores and solid conduction through spherical aerogel particles. Different approaches can be used to obtain the thermal conductivity of a bed of spheres filled with a fluid, which can be categorized into two main divisions: numerical and analytical approaches. Buonanno and Carotenuto [73] used a three-dimensional Finite Element Analysis (FEM) model to calculate the thermal conductivity of simple cubic and body center cubic packed beds. Buonanno *et al*. [74][75] measured the effective thermal conductivity of uniformly-sized rough stainless steel spheres. Their FEM numerical modeling results are in good agreement with the experimental data. Analytical models for calculating the effective thermal conductivity of the packed beds of uniformly sized spheres have been established by Ogniewicz and Yovanovich [76] and Turyk and Yovanovich [77] and verified with experimental data. Bahrami *et al.* [78] also developed a model for predicting the effective thermal conductivity of a packed bed of rough spheres and implemented contact mechanical and thermal analyses to present the results as a compact relationship. Wei *et al.* [79] evaluated the thermal conductivity of silica aerogel powder as an insulation material. They measured gaseous conductivity values from very low pressures up to the ambient pressure and showed its dependence on pressure. In this study, Zehner-Schlunder's [80] modified model for spherical packed beds has been followed to calculate the thermal conductivity of the medium. They assumed that heat transfer occurs through two parallel paths, as they showed in their unit cell: i) the fluid region (air in dry condition (RH=0%) with Kn < 0.1) and ii) solid and fluid regions. Therefore, following [80], the thermal conductivity of the medium is given by Eq.(9):

$$k_m = (1-\frac{1}{R'^2})k_f + (\frac{1-r_s^2}{R'^2})k_{fs} + (\frac{r_s}{R'})^2 k_s \qquad (9)$$

where k_{fs} is the equivalent thermal conductivity of the region that consists of fluid and solid phases, R' is the radius of packed bed unit cell, r_s is the radius of contact area, and k_f and k_s are the fluid and solid (silica aerogel) thermal conductivities, respectively. The unit cell radius, R', is obtained from Eq.(10), in which ε_m is the medium effective porosity, and radius of the contact area, r_s, is determined by Eq.(11); where α is the deformed factor. This parameter is difficult to

measure experimentally, therefore, in this work it is used as a fitting parameter and its value is assumed $\alpha = 0.1$:

$$\frac{1}{R'^2} = \sqrt{(1-\varepsilon_m)} \tag{10}$$

$$r_s = 1 - \frac{1}{(1+\alpha)^2} \tag{11}$$

Assuming that the thermal resistances of the solid and fluid phases are in series with respect to the temperature gradient, the resulting relationship for k_{fs} is:

$$\frac{k_{fs}}{k_f} = \frac{2}{1-\zeta}\left(\frac{1}{1-\zeta}\ln\left(\frac{1}{\zeta}\right) - 1\right) \tag{12}$$

$$\zeta = \frac{k_f}{k_s} \tag{13}$$

ζ is the ratio of fluid thermal conductivity to solid thermal conductivity (k_f / k_s).

Here, the model is modified to include the gas rarefaction effects. Therefore, k_f is defined as following:

$$k_f = \frac{k_{g_0}}{1 + 2\xi Kn} \tag{14}$$

k_{g0} is the gaseous conductivity at STP (p=1atm and T= 298K), which is calculated for dry air as below [50]:

$$k_{air} = 0.00243 + 7.8421\times10^{-5}(T + 273.15) - 2.0755\times10^{-8}(T + 273.15)^2 \tag{15}$$

ξ is a constant, specific to the gas in the pores. It is calculated from the gas accommodation coefficient, α_T, and the specific heat ratio of gas, γ.

$$\xi = \left(\frac{9\gamma - 5}{2\gamma + 1}\right)\left(\frac{2 - \alpha_T}{\alpha_T}\right) \tag{16}$$

For dry air, α_T is 0.8 and γ is 1.4 at room temperature [81]. Kn is the Knudsen number defined as $Kn=\Lambda_m/d_p$, d_p is the mean pore size of the blanket in this work (See Appendix A), and Λ_m is the mean free path of gas molecules in free space, calculated as Eq.(17):

$$\Lambda_m = \Lambda_{m_0} \frac{P_0}{P} \frac{T}{T_0} \tag{17}$$

where Λ_{m0} is in standard condition (69 nm [82]).

Thermal conductivity of the porous medium around the fiber at humid conditions

Actual thermal conductivity of insulation materials is subject to change over time under various environmental conditions. Particularly, insulations may degrade due to moisture absorption or condensation when they are exposed to humidity. Having the proposed unit cell in Section 2.2.1, in a humid environment, pores of the aerogel blanket unit cell would be partially filled with water vapor as well as water droplets. Therefore, the unit cell should be modified as shown schematically in Figure 4. This part presents a comprehensive investigation of aerogel blankets thermal conductivity (k-value) in humid conditions at transient and steady-state regimes.

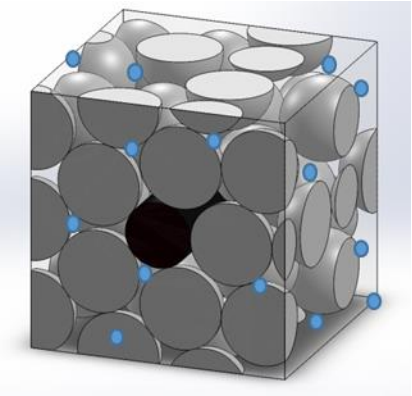

Figure 4. Schematic of the moisture distribution inside the pores of the proposed unit cell; small blue circles depict water droplets.

When an aerogel blanket is placed in a humid environment, it takes hours for moisture to diffuse from the surface of the material to its depth and establish no concentration gradient inside the pores. The reason is that the material shows “resistance” against diffusion of humidity into the pores as well as providing a “capacity” to store moisture inside the pores. This

phenomenon can be described using a well-established resistance-capacitance (RC) model that employs a representative electric circuit to simulate the mass diffusion in aerogel blankets [83].

Modeling a mass transfer in a porous material using an RC model requires finding its equivalent electric circuit. Once the equivalent resistance and capacitance are defined and the circuit is set up, based on the analogous electrical network, the heat and mass transfer phenomena can be modeled using the solution to the electric circuit [84]–[87]. This method is widely used in numerous industrial applications such fuel cell systems [88]–[91]. The proposed zero-dimensional RC circuit (lumped system) for aerogel blanket porous medium is shown in Figure 5 and the equivalent parameters are shown in Table 2-1.

Table 2-1. Table of equivalent parameters in electrical and mass transfer systems.

Electrical system	**Mass transfer system**
Current (I) [=] ampere = coulomb/sec	Water flow rate ($\dot{m}_w$) [=] kg/sec
Potential difference (V) [=] volts	Water vapor concentration (C_w) [=] kg/m^3
Electron charge (Q) [=] coulombs	Moisture content (m_w) [=] kg
Electric capacitance (C) [=] Farad=coulomb/volt	Mass storage capacitance [=] m^3
Electric resistance (R) [=] Ohm= volts·s/coulomb	Diffusion resistance [=] s/ m^3

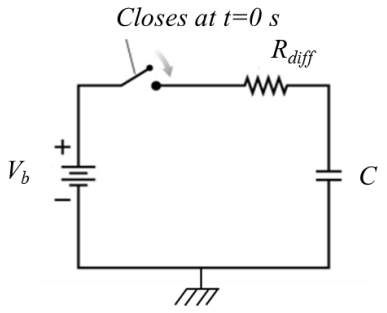

Figure 5. Zero-dimensional (lumped) RC model of aerogel blanket insulation material in humid conditions.

In Figure 5, once the switch is closed at t=0 s, the moisture diffuses into the material and fills up the pores, *i.e.* electrons charge the capacitor till it is fully charged and then the current becomes zero. The resistance against the diffusion of moisture (R_{diff}) is defined following Fick's law and is shown in Eq.(18):

$$R_{diff} = \frac{t_s}{D \cdot A_s} \tag{18}$$

where D is the diffusion coefficient of moisture; and t_s and A_s are thickness and the cross sectional area of the sample, respectively.

Also, C shows the mass storage capacitance of the system that can be calculated using the maximum charge that a capacitor can hold (Q_{max}) and the voltage of the source (V_b) [92]. In this study, the moisture content of the material (m_w) and moisture concentration (c_w) in the porous medium are equivalent to the electron charge (Q) and potential difference (V) in the electrical system, respectively. Hence, having the maximum moisture content of the aerogel blanket samples, which has been measured as discussed in section 2.3.2, the mass storage capacitance can be calculated using Eq.(19):

$$C = \frac{Q_{\max}}{V} = \frac{m_{w\_\max}}{c_w} \tag{19}$$

where m_{w_max} is the weight of the moisture in the sample at steady-state condition. c_w is also calculated assuming water vapor is an ideal gas:

$$c_w = \frac{M_w \cdot P_{sat}}{R \cdot T}(RH) \tag{20}$$

where M_w is the molecular weight of water and R is gas universal constant. P_{sat} is the saturation pressure of water vapor calculated from Eq.(21)

$$P_{sat} = 610.78 \exp(\frac{17.27T + 4717.30}{T}) \tag{21}$$

Therefore, moisture content of the samples over time is calculated using Ohm's law and voltage law for a circuit of series capacitor and resistor, according to Eq.(22):

$$m_w = m_{w\_\max}[1 - e^{-t/\tau}] \tag{22}$$

where τ is the time constant of the system and is calculated as follows:

$$\tau = R_{diff} \cdot C \tag{23}$$

Predicting the moisture content of aerogel blanket materials over time enables us to predict their k-value at any given time under any T and RH condition.

The amount of water droplets, depicted in Figure 4, is assumed to be distributed evenly throughout the medium of the unit cell. Considering that in humid conditions pores include humid air (known RH) as well as water droplets, the medium thermal conductivity of the unit cell, k_m, should be re-defined accordingly:

$$k_{m\_humid} = (1-\sqrt{(1-\varepsilon_{m\_humid})})k_{f\_humid} + \sqrt{(1-\varepsilon_{m\_humid})}(1-r_s^2)k_{fs\_humid} + \sqrt{(1-\varepsilon_{m\_humid})}r_s^2 k_s \quad (24)$$

where k_{m_humid} is the medium thermal conductivity at humid conditions. k_{f_humid} is estimated from Maxwell-Euken model for calculating the thermal conductivity of the mixture of fluids; i.e. humid air as the gas phase (k_g), and water droplets (k_w) [93]:

$$k_{f\_humid} = k_{\mathrm{w}} \frac{2k_{\mathrm{w}} + k_g - 2(k_{\mathrm{w}} - k_g)\varphi_g}{2k_{\mathrm{w}} + k_g + (k_{\mathrm{w}} - k_g)\varphi_g} \quad (25)$$

In Eq.(25), φ_g is the volume fraction of humid air inside the pores, calculated using Eq.(26):

$$\varphi_g = 1 - \varphi_w \quad (26)$$

where φ_w is the volume fractions of water droplets inside the pores, which can be calculated having water content of the samples over time, as is shown in Eq.(27) and Eq.(28). It should be noted that the aerogel materials are super hydrophobic and do not adsorb moisture, i.e. water and humid air fill up the pores.

$$\varphi_w(t) = \frac{u(t)}{\varepsilon_b \cdot V_{dry}} \quad (27)$$

$$u(t) = \frac{m_w(t)}{\rho_w} \quad (28)$$

where $u(t)$ is the volume of the water droplets inside the sample over time, in m^3, and $m_w(t)$ is the moisture content of the sample, in kg. Moisture content modeling over time has been already discussed. ρ_w is the density of water and V_{dry} is volume of the dry blanket.

Thermal conductivity of water is estimated using Eq.(29) [50] :

$$k_w = 0.557 + 0.0022(T + 273) - 1.051 \cdot 10^{-5}(T + 273)^2 + 1.081 \cdot 10^{-8}(T + 273)^3 \quad (29)$$

To calculate the humid air thermal conductivity, Eq.(14) is used and k_{g0} is defined as thermal conductivity of the ideal mixture of water vapor and air at standard condition. It can be calculated knowing the volume fraction of water vapor and air as shown in Eq.(30):

$$k_{g_0} = x_v k_v + (1 - x_v) k_{air} \quad (30)$$

where x_v is the volume fraction of water vapor calculated having RH and T as follows:

$$x_v = RH \frac{P_{sat}}{P_{amb}} \quad (31)$$

where P_{amb} shows the ambient pressure (1 atm). Since volume fraction of vapor is an insignificant value in the considered T and RH, in Eq.(30), the first term is negligible ($x_v k_v$ <<(1-x_v) k_{air}), and k_{g0} can be estimated just by knowing the dry air thermal conductivity ($k_{g0} \approx k_{air}$) (Eq.(15)).

The remaining parameter in Eq.(24), k_{fs_humid}, is calculated having all the defined parameters:

$$k_{fs\_humid} = \frac{2k_{f\_humid}}{1 - \frac{k_{f\_humid}}{k_s}} \left(\frac{1}{1 - \frac{k_{f\_humid}}{k_s}} \ln\left(\frac{1}{\frac{k_{f\_humid}}{k_s}} \right) - 1 \right) \quad (32)$$

Moisture supplement for the thermal conductivity (Z constant)

Effect of the diffused moisture on thermal conductivity of an insulation material is typically reported by the percentage of the difference in wetness levels. According to Ref.[52] and [94] a simple approximate can be used to find the aerogel blanket moisture supplement for the thermal conductivity (Z constant) following Eq.(33):

$$k_{eff\_humid} = k_{eff\_dry}(1 + (\omega Z / 100)) \quad (33)$$

where k_{eff_humid} and k_{eff_dry} are the thermal conductivity of the humidified sample and not humidified sample, respectively. ω is the non-dimensional moisture content (kg/kg) calculated using Eq.(34) following the method will be mentioned in section 2.3.2:

$$\omega(\%) = \frac{m_{wet} - m_{dry}}{m_{dry}} \times 100 \tag{34}$$

Z is the material constant, demonstrates the moisture supplement for the thermal conductivity.

2.2.2. Radiation heat transfer

A portion of heat transfer through aerogel blankets is due to radiation. When a material is optically thick, such as a 1cm thick insulation layer, radiation travels only a short path before being scattered or absorbed. In this situation, radiative heat transfer can be modeled using the Fourier heat conduction law, called the diffusion approximation method [95]. The corresponding thermal conductivity coefficient, k_{rad}, can be found from Eq.(35):

$$k_{rad} = \frac{16\sigma T^3}{3K_R} \tag{35}$$

In this equation, σ is Stefan-Boltzmann constant and K_R is the Rosseland mean extinction coefficient of the blanket. The extinction coefficient shows the deterioration rate of the radiation intensity passing through the material. The Rosseland mean extinction coefficient is defined as Eq.(36) [95]:

$$\frac{1}{K_R} = \frac{\int_0^\infty \frac{1}{\beta_\lambda} \frac{\partial e_{b\lambda}}{\partial T} d\lambda}{\int_0^\infty \frac{\partial e_{b\lambda}}{\partial T} d\lambda} = \int_0^\infty \frac{1}{\beta_\lambda} \frac{\partial e_{b\lambda}}{\partial e_b} d\lambda \tag{36}$$

where λ is the wavelength, T is the medium temperature, e_b is the blackbody emissive power, $e_{b\lambda}$ is the spectral black body emissive power, and β_λ is the spectral extinction coefficient. The extinction coefficient, which represents the scattering and absorption, is a key parameter in radiative heat transfer models. The extinction coefficient can be found either by analytical models based on the type and morphology of fibers or from experimental methods. The

experimental approach uses the measured transmittance spectrum from a FTIR spectrometer to calculate the extinction coefficient. The spectral extinction coefficient for a thin sample can be obtained using Beer's law [95].

$$\beta_\lambda = -\frac{\ln(T_{n\lambda})}{t_s} \tag{37}$$

$T_{n\lambda}$ is the spectral transmittance and t_s is the thickness of the sample. In this study, the spectral transmittance was measured for two types of aerogel blankets for the wavelength range of 2.5–40 μm (Figure 6) using a FTIR spectrometer (Shimadzu- IR Prestige-21 model).

Finally, presented in Eq.(38) is the final relationship for the effective thermal conductivity of the aerogel blanket at dry or humid conditions obtained by superposition of the conduction and radiation thermal conductivities following [70]:

$$k_{eff} = k_{cond.} + k_{rad.} \tag{38}$$

2.3. Experimental study

In this research, samples of aerogel blanket produced by two manufacturers, Aspen Aerogel Inc. and Cabot Aerogel Corp., are investigated. Table 2-2 shows the specifications of the samples in terms of what manufacturers reported and what were tested in this study.

Table 2-2. Aerogel blanket samples specifications

Manufacturer Data [60, 61]

Sample	Provider	Thickness	Density*	Fiber composition	Powder material	Thermal* Conductivity
Cryogel® Z (CZ)	Aspen Aerogel	10 mm 5 mm	130 kg·m^{-3}	Polyester/ fiber glass	Silica (SiO_2)	0.014 W·m^{-1}·K^{-1}
ThermalWrap™ (TW)	Cabot Corp.	8 mm 5 mm	70 kg·m^{-3}	Polyester and polyethylene	Silica (SiO_2)	0.023 W·m^{-1}·K^{-1}

Measured Values

Sample	Particle diameter	Fiber Diameter	Porosity	Extinction coefficient
CZ	10 μm	20 μm	91%	4014 m^{-1}
TW	4 μm	7 μm	79%	3165 m^{-1}

*At room temperature

The extinction coefficients of both aerogel blanket samples were determined from their spectral transmittance (measured using a FTIR spectrometer) which are shown in Figure 6 (a) and (b). The extinction coefficients were subsequently calculated by Eq.(36).

The porosities of the samples were measured by the MIP method using a mercury intrusion porosimeter (AutoPore IV, Micromeritics Instrument Corporation).

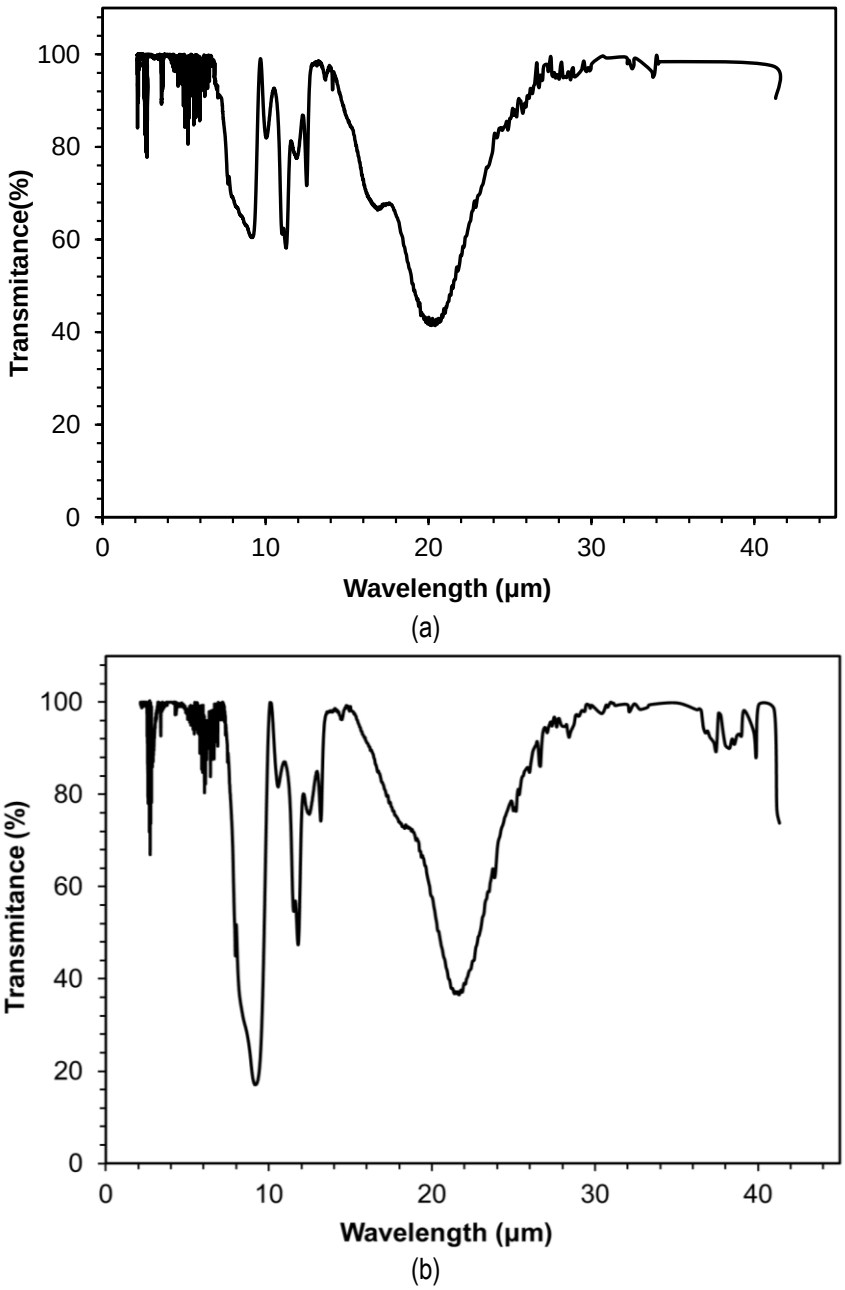

Figure 6. Spectral transmittances of (a) CZ, and (b) TW.

2.3.1. Thermal Conductivity Measurements of the Dry Samples

The heat flow meter (HFM) method is based on establishing a steady-state, 1-D heat flux through a test specimen. In Figure 7, Netzsch HFM 436 Lambda, which is used for measuring the thermal conductivity of dry insulation samples (0.002 to 2 $W \cdot m^{-1} \cdot K^{-1}$) is shown. The instrument has been calibrated with a NIST-certified reference standard of known thermal conductivity. The tests were conducted as per ASTM C518 standard. The sample, 30.5 cm × 30.5 cm, with thicknesses ranging from 5 to 10 mm, were sandwiched between two metallic plates with a controlled temperature gradient, and mechanical load (pressure) control. The allowable range for implementing thermal conductivity tests using this device is -40 to 100˚C (on the plates), therefore, in the present study, tests were performed with mean temperatures ranging from -20 to 80˚C, temperature gradients of 40˚C, and fixed pressure load of 0.5 Psi following ASTM C177. In HFM, sensors measure the heat flux and thermocouples measure the hot and cold plate temperatures. The HFM signal, Q (μV), is proportional to the heat flux $\dot{q}$ across the sample, which is proportional to the temperature difference, ΔT, between the plates and inversely proportional to the total thermal resistance, R_{tot}:

$$\dot{q} = -k\frac{\Delta T}{\Delta x} = \frac{\Delta T}{R_{tot}} \tag{39}$$

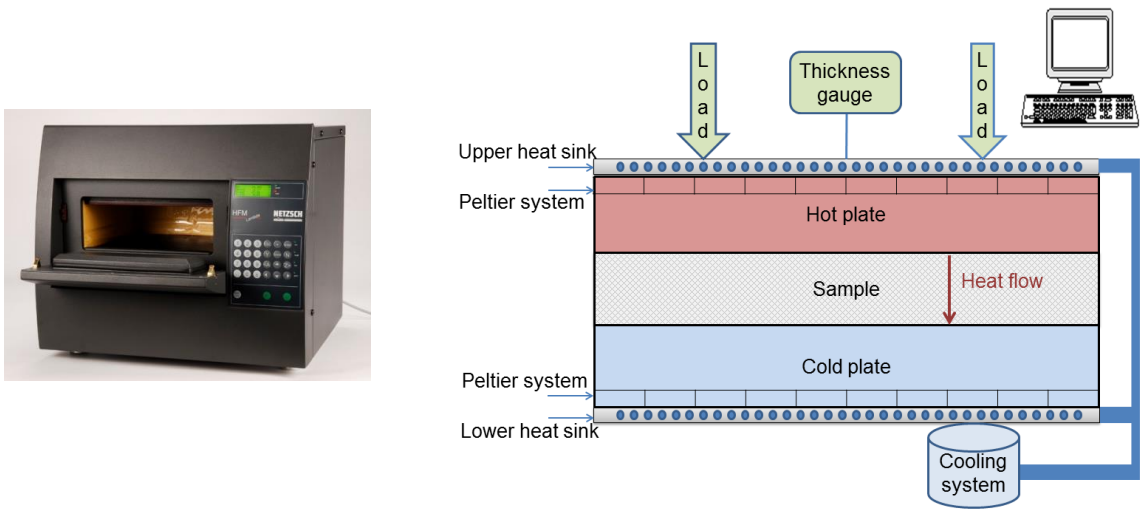

(a) (b)

Figure 7. (a) The HFM instrument, and (b) its schematic.

2.3.2. Moisture Content Measurements

Moisture content prediction is a laborious task mainly due to the slow diffusion of moisture through porous materials, which makes the experimental study particularly long. In this study, water uptake of the aerogel blanket samples were measured following the ISO 12571:2013 Standard (Hygrothermal performance of building materials and products – Determination of hygroscopic sorption properties, Part B- climatic chamber method) [94]. Samples were placed in an environmental chamber, ESPEC Platinous series EPX-4H, capable of recreating a wide range of temperature (10°C-85°C) and RH (0-98%) conditions. They were exposed to 0%, 40% and 90% RH at temperatures of 25°C and 45°C for 24 hours wetting process. Weights of the samples were measured after each wetting period, using Ohaus Adventurer^{TM} Balance having 0.0001g standard deviation. Prior to moisture sorption tests, the samples were dried, for 24 hours (according to our measurements the equilibrium was reached after 24 hours and the samples were completely dried), at 70°C under normal atmospheric pressure, and weighed to calculate the weight change after each wetting time. 70°C is safe, as the maximum possible temperature that the insulation materials can be used at is reported to be 125°C by the supplier [96], [97], and this temperature does not affect their physical and chemical structure.

2.3.3. Thermal conductivity Measurements of the Samples at Different Levels of RH

Thermal conductivity measurements at higher levels of RH were performed as per ISO22007-2[98], using a transient plane source (TPS) thermal constants analyzer (TPS 2500S, ThermTest Inc., Fredericton, Canada). The temperature controlled chamber was modified to create an input and exit port for the flow of air with controlled humidity and a humidity sensor was added to the chamber. The flow of humid air was provided by a Cellkraft F-series humidifier. The humidifier operates through water transfer across a perfluorinated sulphonic acid membrane and is suitable for accurate humidity control without droplets. It can measure the gas temperature with ±0.2ºC accuracy in the range of 0 to 50ºC and ±1.7% for RH between 0 to 90%, i.e., the range used in this study. The temperature of the flowing humid air was matched to the temperature in the chamber. The flow rate was 6 nlpm (nominal litres per minute) with the RH under feedback control using the sensors within the chamber and the humidifier.

TPS device has several “hot disk” two-sided sensor types and software modules to conduct measurements on bulk materials (isotropic and anisotropic), thin films, powders and liquids. In this work, a sensor (TPS Hot Disk 7577) with a 2.001 mm radius nickel double spiral insulated in a thin layer of Kapton was used for simultaneous transient heating of the sample and precise temperature measurement. For bulk measurements, the sensor was placed between a pair of identical samples of 5 cm × 5 cm × 5 mm and compressed using a standard weight to minimize the thermal contact resistance. The sample-sensor assembly is shown in Figure 8. Each test was repeated three times to ensure the repeatability of the results. Low standard deviation of the measured data (about 2×10^{-4} $W\cdot m^{-1}\cdot K^{-1}$) shows the reliability of the collected data. More details of the methodology used in the thermal conductivity measurements can be found in Ref. [99].

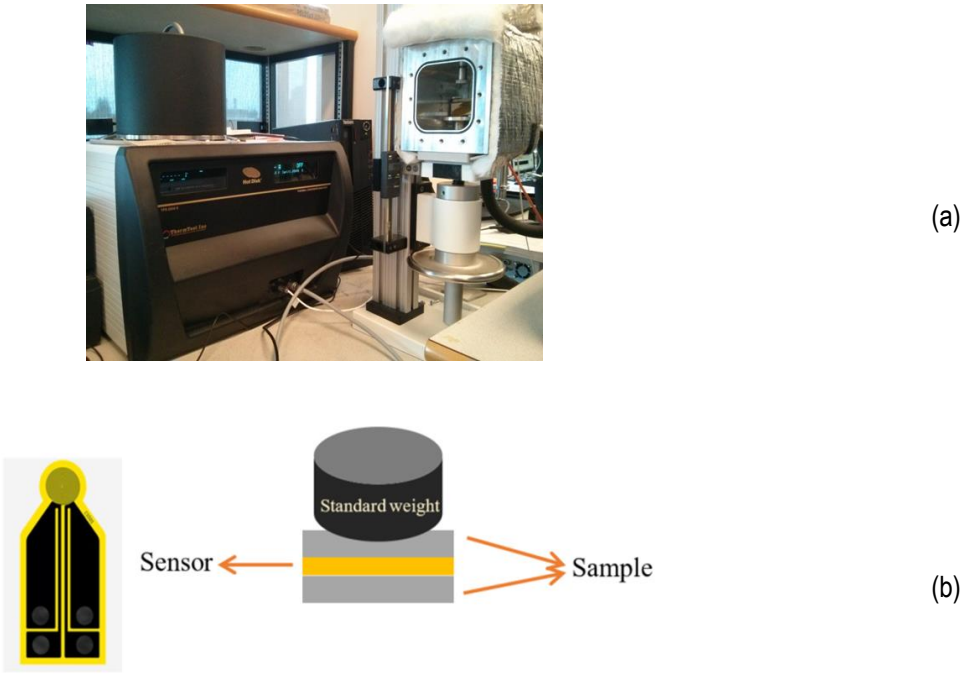

Figure 8. Device (a) and simplified schematic of TPS (Transient Plane Source) thermal conductivity measurement (b).

2.4. Results and Discussion

The proposed mathematical model was solved using MATLAB [100], which enables parametric studies and analysis. In the following section, a comparison of modeling results and the experimental data is provided, followed by parametric studies in which the effects of variable parameters on the effective thermal conductivity of aerogel blanket are examined.

2.4.1. Model Validation and Parametric Studies for the Dry Samples

The test conditions mentioned in section 2.3.12.3 were applied to the samples of aerogel blanket. It was detected that aerogel blanket samples spread fine particles of silica dust during the measurement of k-value using HFM. Four original dry aerogel blanket samples were placed in and removed from the HFM multiple times and the thermal conductivities of these samples were measured for each placement/removal. The results specified that the handling does not contribute in changing the k-value. Consequently, each sample is tested for three times with the same temperature conditions; the standard deviations are less than $10^{-3}\,W\cdot m^{-1}\cdot{}^{\circ}C^{-1}$.

Presented in Figure 9, good agreement was observed between the experimental and modeling results of the effective thermal conductivity variation of dry CZ and TW over a temperature range of -20 to 80°C. The highlights of Figure 9 are:

- Higher temperature leads to higher thermal conductivity;
- By increasing the temperature from -20 to 80°C, the effective thermal conductivity increases approximately 12% for CZ and 44% for TW, which is due to higher radiation and gas conduction heat transfers for TW compared to CZ; and
- The effective thermal conductivity of CZ is less than TW, which was consistent with manufacturer data sheet. It can be because of lower thermal conductivity of fibers and smaller blanket pore sizes in this composite.

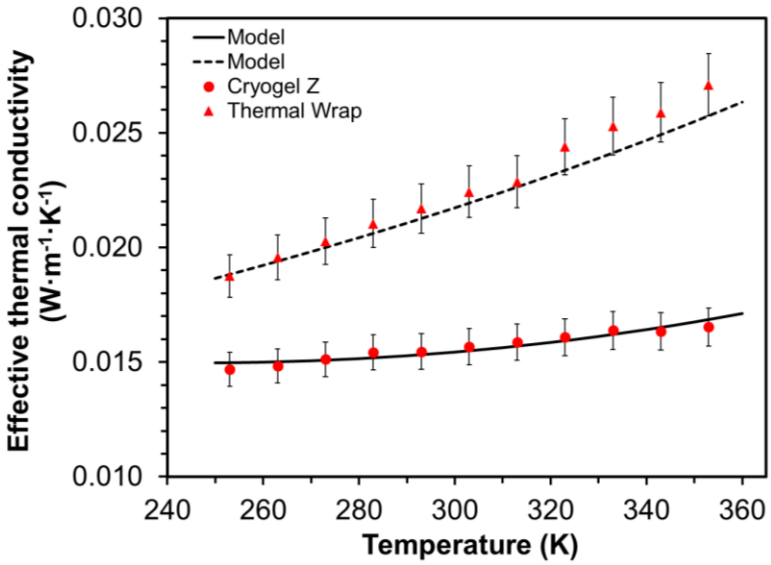

Figure 9. Temperature dependence of the thermal conductivity of dry CZ and TW aerogel blankets.

Figure 10 shows a comparison of the contribution for each heat transfer mode in the effective thermal conductivity of CZ and TW. It reveals that the major portion (about 95%) of the total thermal conductivity is due to the conduction (gas and solid). It should be noted that this contribution decreases with increasing temperature because the radiation contribution rises and this effect is more prominent in TW samples.

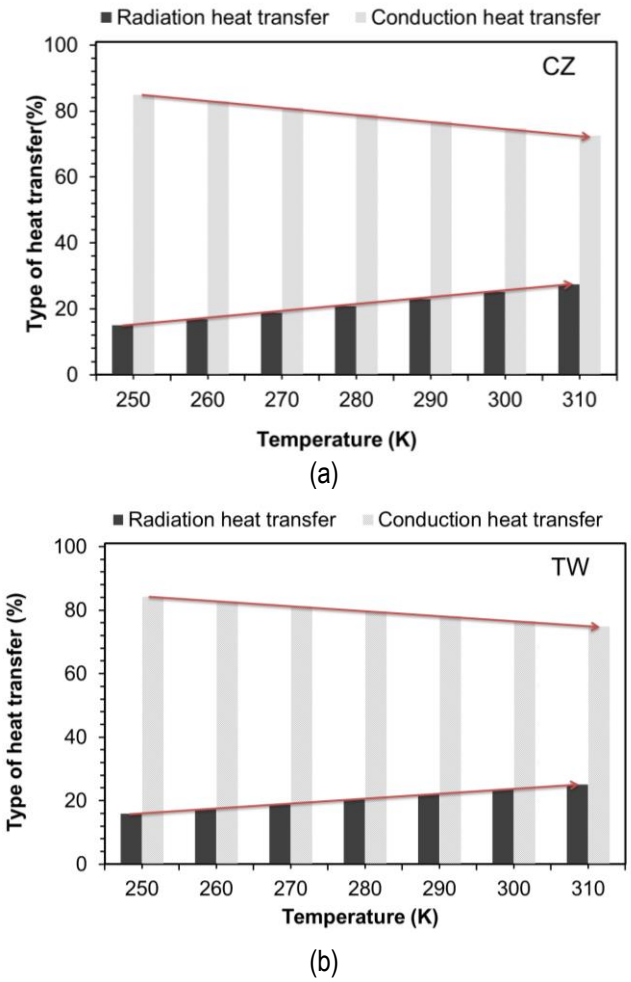

Figure 10. Contribution of each type of heat transfer (%) on total heat transfer rate; (a) CZ, and (b) TW.

The developed model can be conveniently used to systematically study the effect of aerogel blanket microstructural parameters, thermophysical properties, and operating conditions on its effective thermal conductivity. The important parameters that produce noticeable variations in the effective thermal conductivity are fiber thermal conductivity and porosity of the blanket. The objective is to investigate optimized values for such parameters, which can lead to new designs of aerogel composites with lower effective thermal conductivity. As shown in Figure 11, fibers thermal conductivity, as one of the influential factors in the aerogel blanket structure, has a minor effect on the effective thermal conductivity of the blanket, keeping the other parameters constant. This analysis provides more appropriate options for choosing low thermally conductive fibers along with the cost and availability.

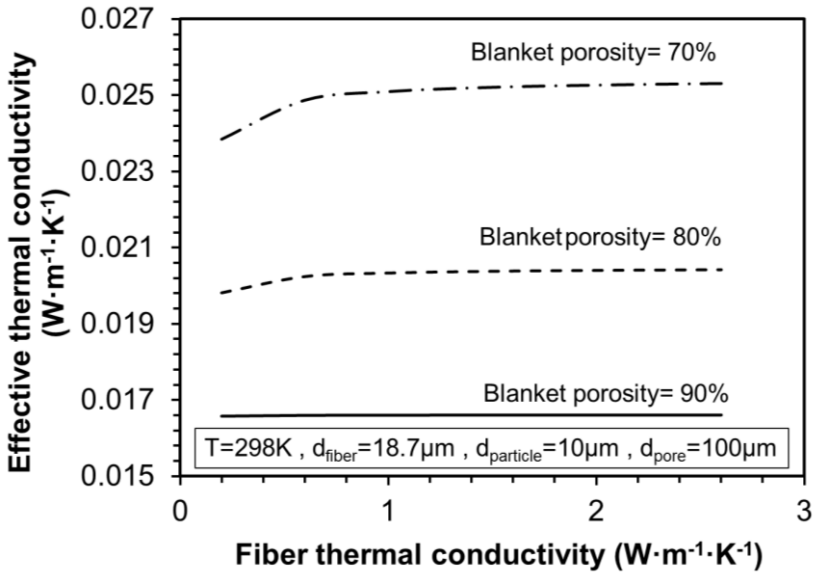

Figure 11. Effect of fiber material thermal conductivity on the effective thermal conductivity

Figure 11 highlights are:

- The lower the blanket porosity, the higher the effective thermal conductivity; and
- By decreasing the blanket porosity from 90% to 70%, the thermal conductivity increases about 40%, which is prominent.

It should be noticed that high blanket porosity can be interpreted as a few large pores or lots of small pores. Larger pore sizes create larger gaps which leads to having convection heat transfer and more conduction through gas molecules and the effective thermal conductivity increases when there are larger pores in the blanket. On the other hand, larger pore sizes result in higher porosity which might be a factor for less effective thermal conductivity. This issue is addressed in aerogel blanket by creating large surface areas in combination with nano-porous pathways. Hence, high porosity and small pore sizes are keys to low thermal conductivity in aerogel blankets.

Low thermal conductivity in aerogel blankets is due to its nature as a highly porous solid material, which means almost no gas convection, very small gas and solid conduction, and small radiation heat pathways. Hence, as it can be understood from Figure 12, reducing the porosity eliminates the leverage of using aerogel blankets as an insulation material and in this case, using the other conventional types of insulations may be more prudent.

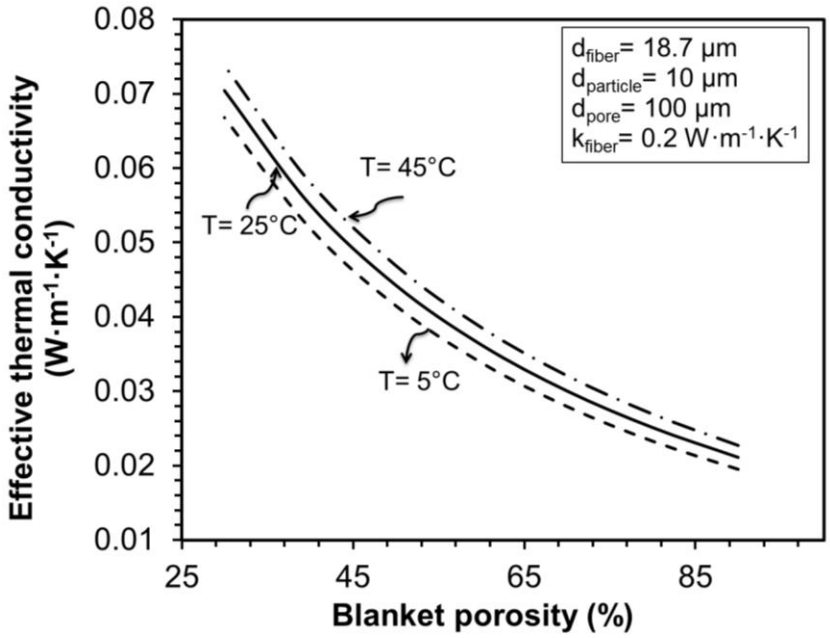

Figure 12. Effect of blanket porosity on the effective thermal conductivity.

Additionally, the effect of temperature history on thermal conductivity of the available samples was investigated. A fixed, periodic temperature of -20 and 80°C, was applied on each sample for 20 cycles. As it is shown in Figure 13 and Figure 14, k-value variation was stable during all the cycles and peek to peek thermal conductivity values stayed constant. Therefore, it can be concluded that 100°C temperature variation definitely affects the k-value, however, accelerated temperature variation from -20 to 80°C does not have any destructive effect on thermal performance of aerogel blanket samples.

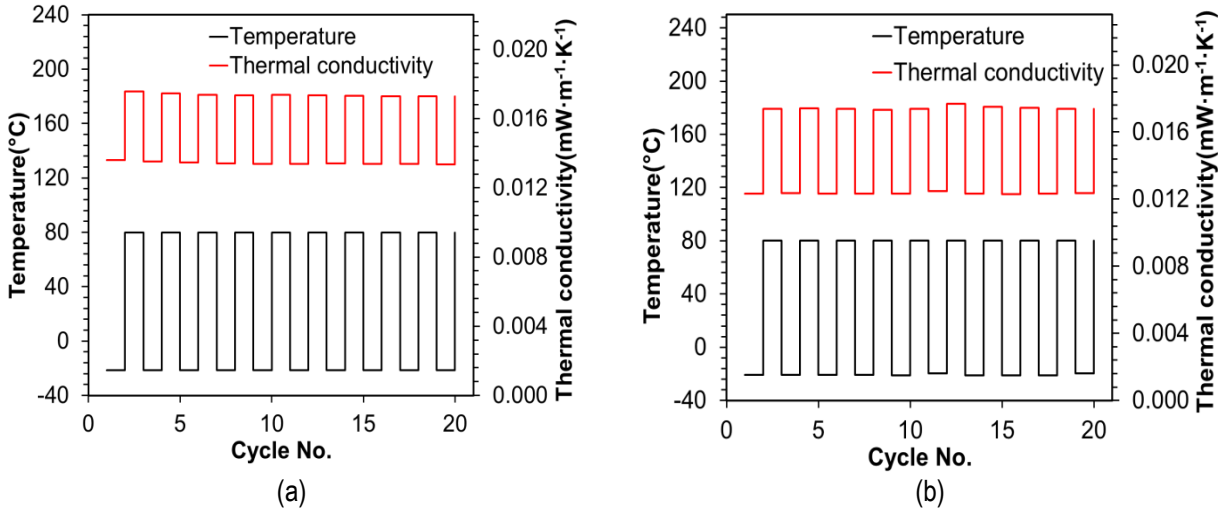

Figure 13. Thermal conductivity variation during temperature cycling for CZ, (a) 10mm, and (b) 5mm thickness.

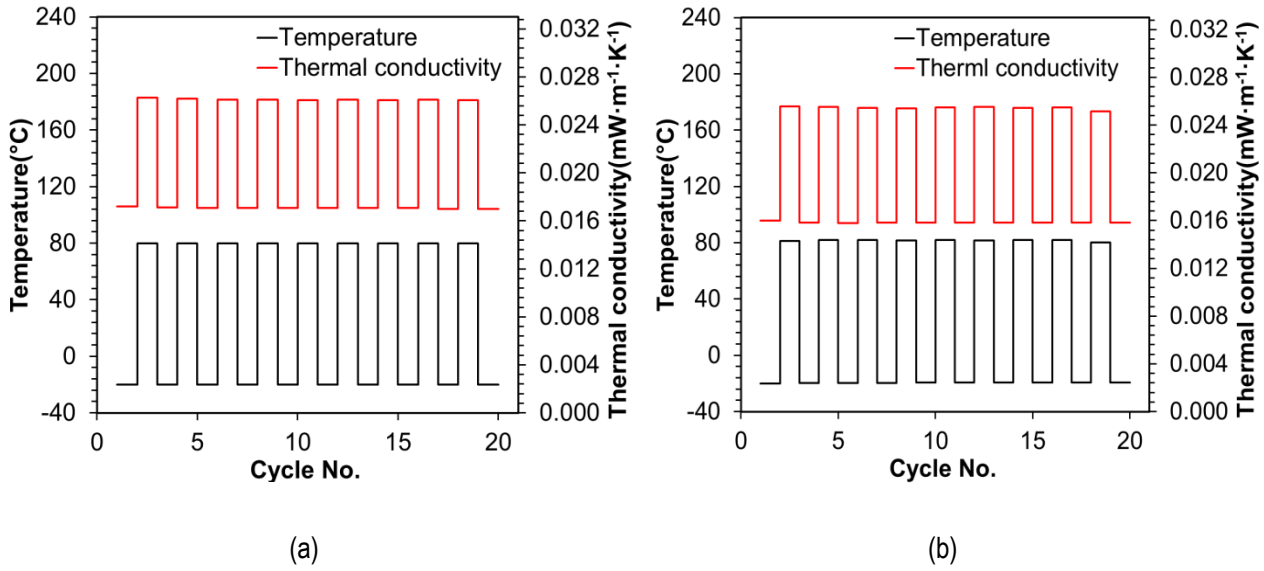

Figure 14. Thermal conductivity variation during temperature cycling for TW, (a) 8mm, and (b) 5mm thickness.

2.4.2. Model Validation and Parametric Studies for the Samples at Different Levels of RH

Sorption isotherm measurements

Sorption isotherms (the moisture taken up from the air as a function of RH), is one of the important characteristics of materials. Due to the complexity of sorption processes, isotherms cannot be calculated theoretically and should be measured experimentally for each material [52]. Figure 15 shows the sorption isotherms for the samples of aerogel blanket at two different temperatures to see the effect of temperature on moisture content as well. The error bars show the standard deviation of the measurements. The plots demonstrate that increasing humidity and decreasing temperature increase the moisture content. Furthermore, the maximum amount of moisture uptake is 2.87% of dry mass for TW and 2.34% of dry mass for CZ measured at 25°C. Figure 16 clearly shows that the observed weight increase in the samples after wetting is due to water droplet formation inside the pores, i.e., if all the pores were filled with water vapor (at a given RH and T), the weight increase of the samples would be order of magnitudes less than the measured values. Therefore, weight of the water vapor has been neglected in the modeling section, compared to the liquid water, and the defined moisture content (m_w) just shows the weight of the water droplets.

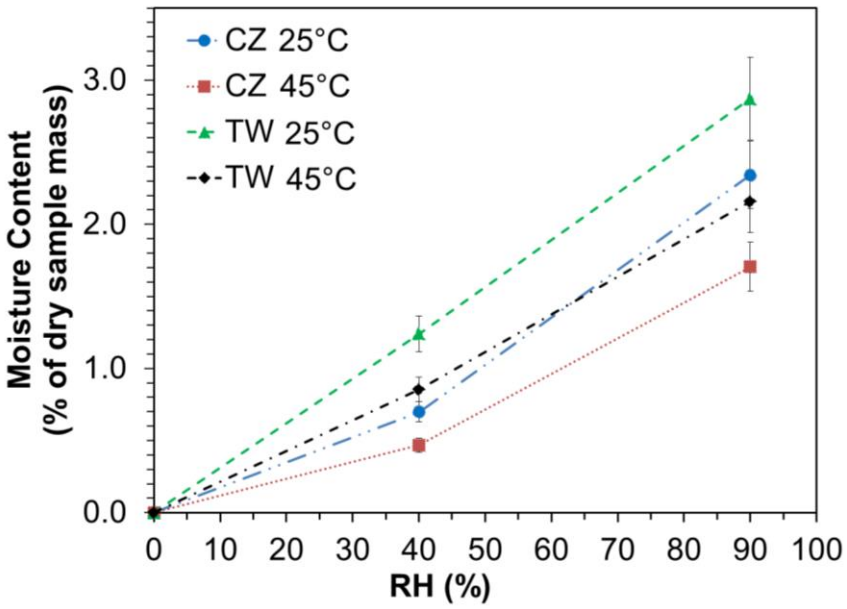

Figure 15. Sorption isotherms at 25°C and 45°C for CZ and TW aerogel blanket samples.

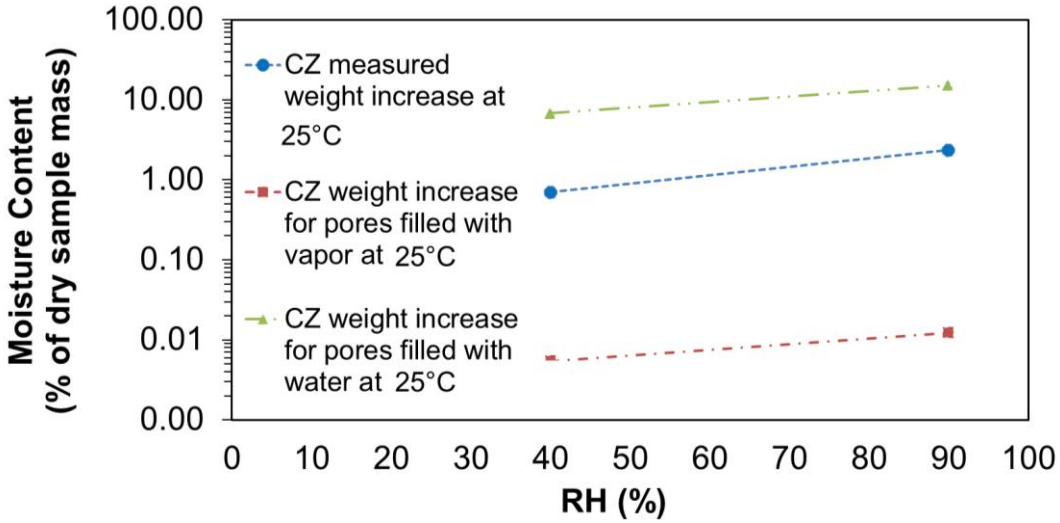

Figure 16. CZ weight increase in three cases: blue line: actual measured data; red line: water vapor filled the pores; and green line: liquid water filled the pores.

Thermal conductivity analysis at the transient regime

For each aerogel blanket type, two 5 mm thick pairs of 5 cm × 5 cm square samples were prepared to be tested at different levels of RH and temperature using our TPS-humidifier assembly. Cyclic thermal conductivity measurements of aerogel blankets were performed between 0% and 80% RH, with power of 10 mW and measurement time of 40s in short intervals. In Figure 17, each data point was measured after 5 hours rest time, after changing the

humidity condition. The measured data revealed that thermal conductivity was increased over time, at cycles with the same RH. This can be interpreted as a result of moisture buildup inside the pores. It also shows that it should take more than 5 hours for the moisture to leave the pores. Besides, it is observed that after approximately six cycles, the effective thermal conductivity reaches its maximum, which means the material was holding all the humidity that it could.

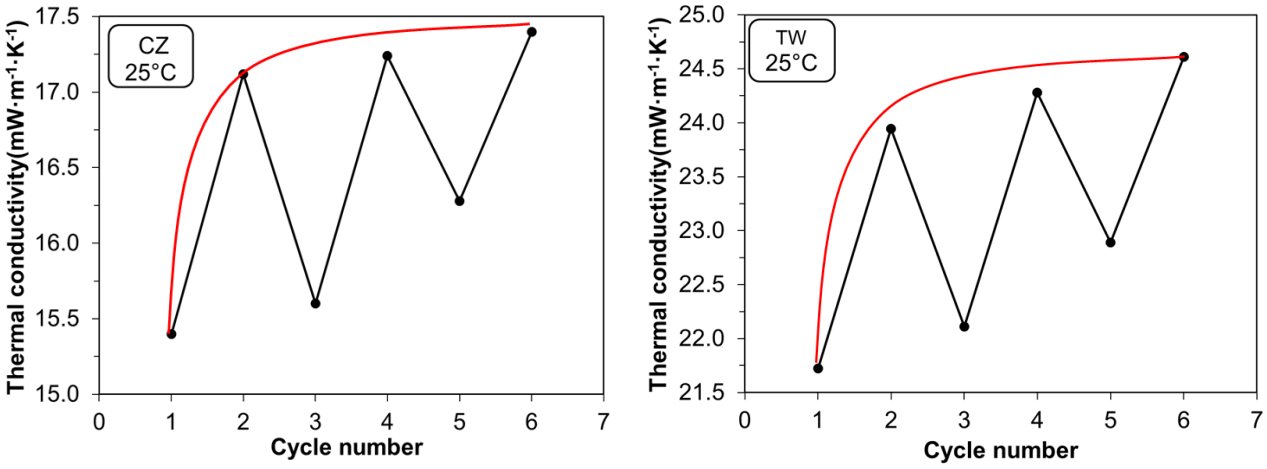

(a) (b)

Figure 17. Cyclic thermal conductivity measurements of CZ and TW between 0% and 80% RH at 25°C.

To find the diffusion coefficient (*D*) defined in Eq.(18), a series of long-term experiments on CZ were performed using TPS-humidifier assembly. The dry sample of CZ was placed inside TPS at 25°C, under fixed conditions of 20%, 40% and 80% RH for more than a month and the thermal conductivity was measured at different time intervals from 5 hours to weeks to ensure that steady-state was reached. Before each set of measurements, the dry sample was tested for 24 hours at 0% RH, in different time intervals to ensure that its thermal conductivity remains constant over time.

Genetic algorithm optimization method (with the parameters of: population size of 50, generations and selection rate of 100%, migration rate of 10% and mutation rate of 90%) [42] was applied on the data set of 80% RH, to obtain the appropriate diffusion coefficient (*D*) of CZ. The objective function is shown in Eq.(40):

$$min \quad error = sum(k_{eff\_humid\_model}(t) - k_{eff\_humid\_data}(t))^2 \tag{40}$$

The fitted value of *D* was used for modeling the moisture content of CZ at any other RH condition following Eq.(22). Since the model accurately predicts the data set of 20% and 40% RH, as shown in Figure 18, the fitted value of *D* is reliable. A sensitivity analysis on the typical values of *D* is presented in Figure 19 for three times after changing the RH to 20%, i.e., 1 hour, 10 hours, and 25 hours. It shows that changing *D* in the range of 10^{-10} to 10^{-6} m^2s^{-1} changes the effective thermal conductivity less than 2%. It also demonstrates that at the beginning of the diffusion process (t=1 hr), the diffusion coefficient has a stronger effect on the effective k-value compared to the steady-state condition.

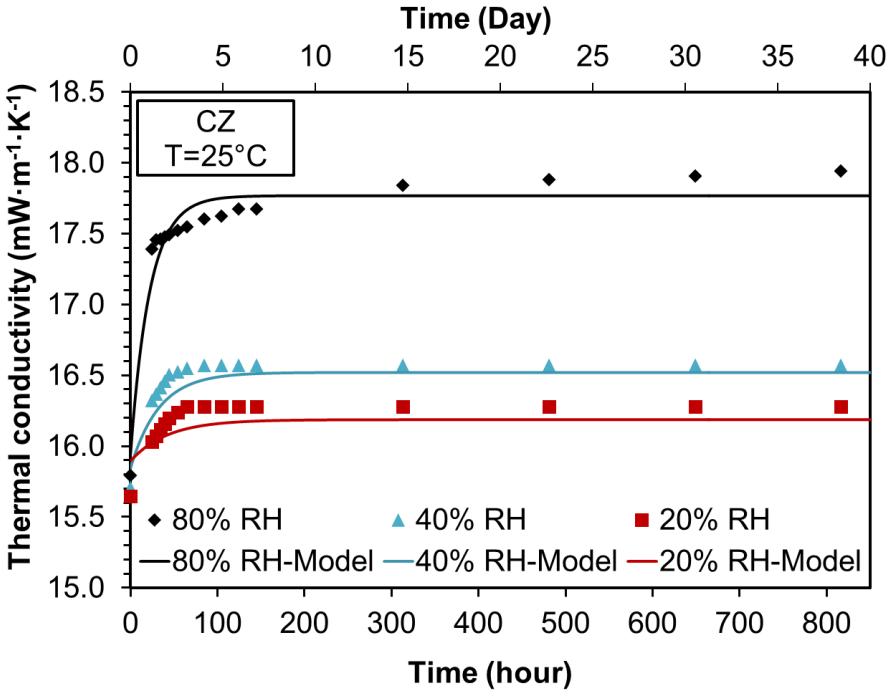

Figure 18. Thermal conductivity of CZ over time at 25°C and 20%, 40% and 80% RH.

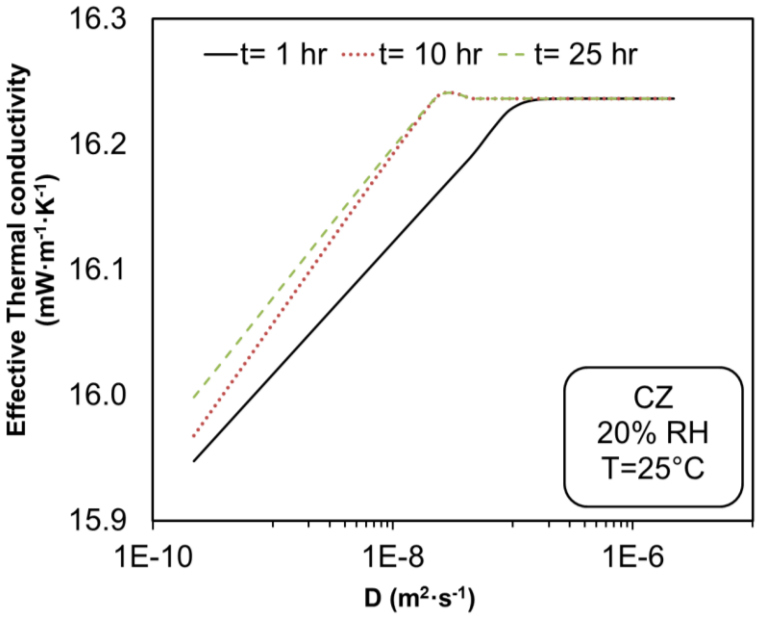

Figure 19. Sensitivity analysis on CZ diffusion coefficient at 20% RH and 25°C.

Figure 18 shows that it took about 20 hours for thermal conductivity of CZ at 80% RH to reach steady-state condition, which is due to the diffusion resistance and storage capacitance of the sample. Water volume fraction increase (percentage of the pore volume) is also shown over time in Figure 20, which indicates that in a humid environment, moisture gradually replaces air in the pores until no concentration gradient throughout the sample exists.

Values of diffusion coefficient (D) and time constant (τ) are shown in Table 2-3. As it is shown in this table, it takes more time for CZ to reach to steady-state condition at higher RH, because of the higher vapor partial pressure gradient between the dry aerogel and ambient at higher RH.

Table 2-3. Diffusion parameters of CZ at different RH.

	20% RH	**40% RH**	**80% RH**
D ($m^2 \cdot s^{-1}$)	2.2×10^{-9}		
τ (hours)	12.37	14.00	19.59

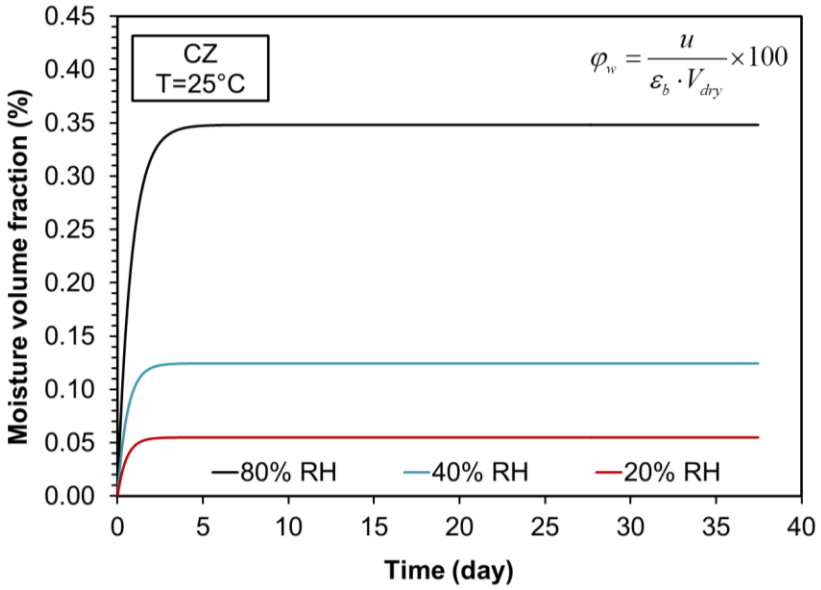

Figure 20. Moisture volume fraction of CZ over time at 25°C.

Thermal conductivity analysis at the steady-state regime

The thermal conductivity of each pair of samples was measured in TPS-humidifier assembly with a power of 10 mW, measurement time of 40 s and the rest interval of 24 hours between measurements to ensure steady-state condition is reached. Figure 21 and Figure 22 present the effective thermal conductivity of aerogel blanket samples as a function of RH at two temperatures of 25°C and 45°C.

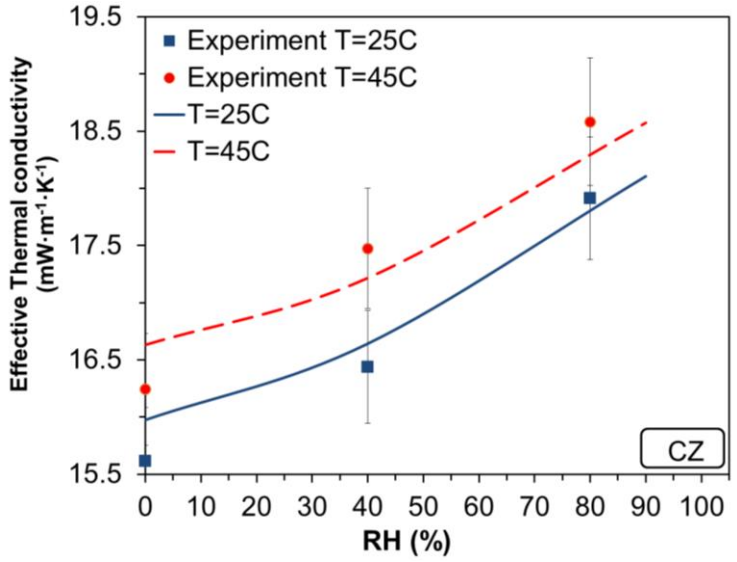

Figure 21. Effective thermal conductivity as a function of RH for CZ at 25°C and 45°C.

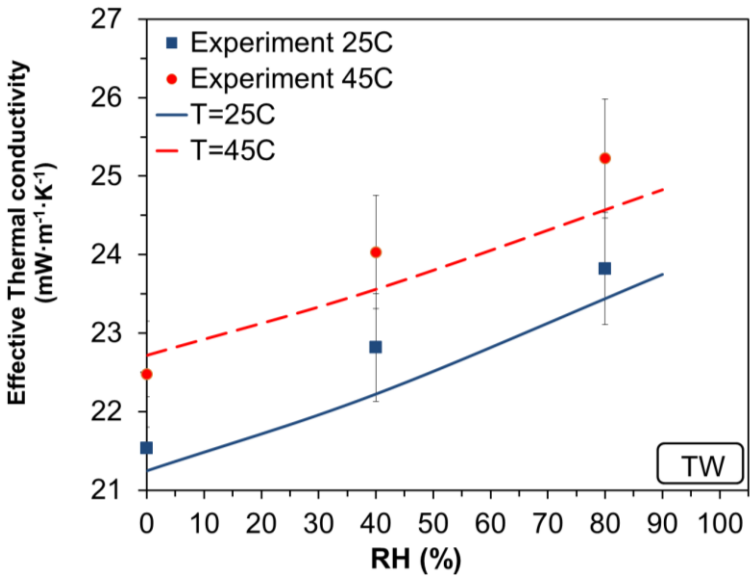

Figure 22. Effective thermal conductivity as a function of RH for TW at 25°C and 45°C.

Results show that increasing the RH from 0% to 90% increases the k-value ~14% for CZ and ~11% for TW after reaching steady-state. This thermal conductivity increase is a result of liquid droplet accumulation inside the pores at higher RH that replaces the dry air and results in higher heat transfer rate inside the material. Also, according to Figure 21 and Figure 22, the modelling results at 25°C and 45°C (the solid and dash lines) become closer at higher RH. The reason is that having more moisture content at the lower temperature (See Figure 15) leads to a slightly sharper thermal conductivity increase at 25°C.

Chapter 3.

Aerogel Blanket Mechanical Deformation Analysis

Silica aerogel tend to crack after repeated usage, which affect the long-term performance of the aerogel blanket insulation materials, in terms of porosity, thickness, and thermal resistance. Therefore, the mechanical behavior of aerogel blankets under compression should be understood. In this research, the mechanical performance of two types of aerogel blanket samples under compression and after repeated cycling load is studied. Additionally, the proposed unit cell approach in the previous chapter is modified to develop a mechanistic analytical model for predicting the compressive stress-strain relationship of aerogel blankets. In this model, only aerogel blankets microstructural properties, such as fiber and particle diameters, elastic modulus, and porosity are used. Bending of fibers is considered as the main deformation mechanism at the unit cell level and overall blanket deformation is calculated from the summation of the deformations of all the unit cells. Employing the proposed model, the stress-strain relationship is presented and verified using the experimental data.

3.1. The Present Model

SEM images of the aerogel blankets revealed a repetitive microstructural arrangement of fibers and aerogel particles leading to a unit cell approach for the analytical model. Figure 23 (a), (b), and (c) show a SEM image of a CZ aerogel blanket, schematics of the proposed geometric model and the unit cell which is a modified version of the propose unit cell in section2.1.4, respectively. This unit cell, designed to model the mechanical behavior of aerogel blanket under compression, includes fibers surrounded by small aerogel particles with a large particle at the center. Each fiber is modeled as a bending beam supported through a contact point with the fiber below. Force is applied to each fiber through a contact point with a fiber above that is one edge of the unit cell, l_{fiber}, away from the supporting contact point.

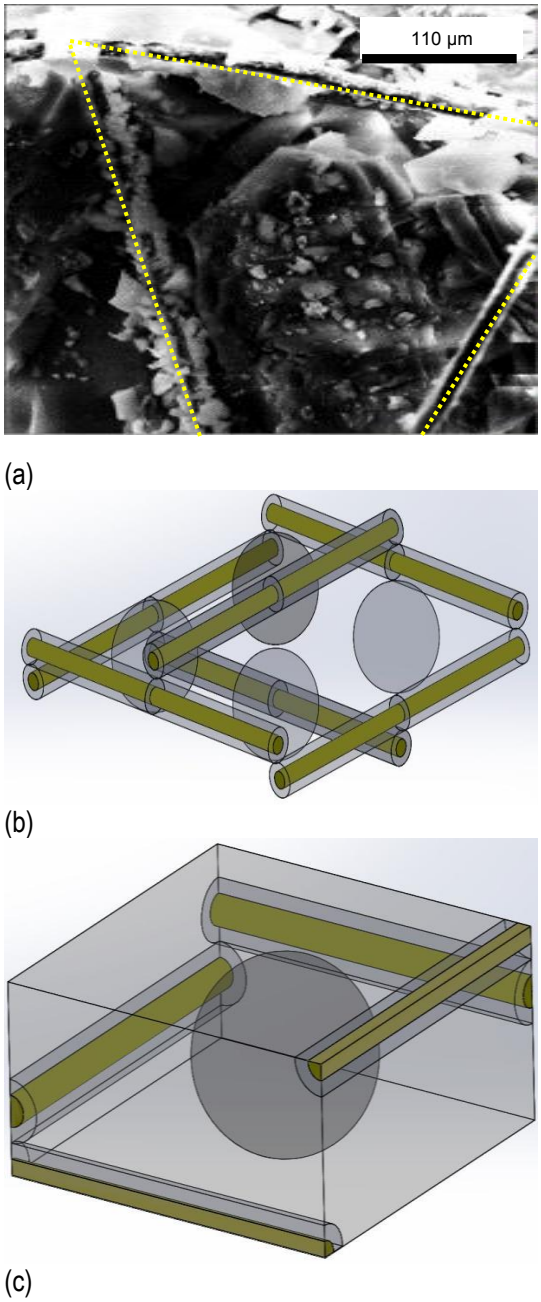

Figure 23. (a) SEM image of aerogel blanket (CZ) showing aerogel coated fibers (marked with dotted lines) and aerogel filled pores, and (b) schematic of the proposed geometrical model for aerogel blanket, and (c) schematic of the unit cell showing fibers coated with a layer of aerogel particles, a larger spherical aerogel particle at the center, a force, F', applied to the uppermost fiber and the fibers length in the unit cell, l_{fiber}.

In our approach, two different porosities were considered: 1) porosity of the aerogel coating on the fibers, ε_a; and 2) porosity of the blanket, ε_b. The assumptions used in the model development are listed below:

1. Smooth sphere and fiber surfaces, *i.e.*, no rough contacts on sphere-sphere and fiber-sphere contact points;

2. No contact point between the large particle at the center and the fiber-aerogel composite, *i.e.*, the unit cell aspect ratio is $l_{fiber}/D_{lp} \geq 2$. For this assumption to be applicable, the range of the applied load should be limited to less than 10 kPa, that is in the range of the load applied on such material in practice; and

3. Negligible deformation for aerogel particles (Hertzian contact), compared to bending fibers deformation ($\delta_{max\_fibers} \sim 10^{10}\ \delta_{max\_particles}$).

The length of the fibers in each unit cell, l_f, is equivalent to the length of the two edges of the unit cell, and can be found from the porosities using the following equation:

$$1-\varepsilon_b = \frac{V_{solid}}{V_{tot}} = \frac{\frac{3\pi}{8} {D_{fiber}}^2 l_f + \frac{3\pi}{2} l_{fiber}\left(D_{fiber} t_a + {t_a}^2\right)\left(1-\varepsilon_a\right) + \frac{4\pi}{3}\left[3\left(\frac{D_{fiber}}{2}+t_a\right)\right]^3\left(1-\varepsilon_a\right)}{6{l_{fiber}}^2\left(\frac{D_{fiber}}{2}+t_a\right)} \quad (41)$$

where V_{solid} is the solid volume of the unit cell, V_{tot} is the total volume of the unit cell, D_f is the diameter of the fibers, and t_a is the thickness of the layer of aerogel on the fibers, which is assumed to be equal to an aerogel particle diameter. The third edge of the unit cell can be calculated from the fibers and aerogel layer thickness ($3\times(D_{fiber}+2t_a)$). From the length of the fibers and the compressive force, which is assumed to be applied on the end point of the fiber on top, the deflection of the unit cell in the *z* direction can be calculated according to the beam theory for beams supported on both ends and single load at the center, Figure 24(a) [101]. Also, according to the second and third modeling assumptions, the large spherical aerogel particles are only contributing to the effective porosity of the unit cell and do not affect the total deformation, so the stress-strain analysis is applied on the simplified unit cell, as shown in Figure 24(b).

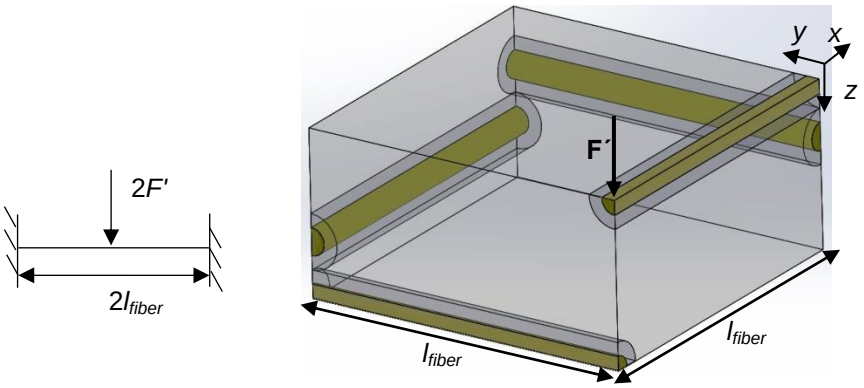

(a) (a)

Figure 24. (a) Schematic of the applied beam theory, and (b) the unit cell used in stress-strain analysis.

The unit cell deflection is calculated from Eq.(42):

$$\delta_u = 4 \times \delta_{Beam} \tag{42}$$

where the deflection of each beam, δ_{Beam}, is

$$\delta_{Beam} = \frac{F' \times l_{fiber}^{\ 3}}{3(EI)_{eff}} \tag{43}$$

the applied force on one unit cell is:

$$F' = \frac{F_{tot}}{N_u} \tag{44}$$

and N_u is the number of unit cells in one layer, obtained using the equation:

$$N_u = \frac{A_{sample}}{l_{fiber}^{\ 2}} \tag{45}$$

in which A_{sample} is area of the sample. $(EI)_{eff}$ is the effective flexural rigidity of the beam, which can be calculated using elastic modulus of fibers and aerogel particles, E, and their moment of inertia, I , according to Eq.(46):

$$(EI)_{eff} = (EI)_{fiber} + (EI)_{aerogel} \tag{46}$$

However, the *EI* term corresponding to aerogel layer is negligible compared to fibers elasticity, thus, is not considered in the model.

To calculate the total deformation of an aerogel blanket, the number of layers should be multiplied by the deformation of one layer, which equals the deformation of one unit cell ($\delta_{layer} = \delta_u$). The number of layers in the through-plane direction can be calculated from:

$$N_{layers} = \frac{t_b}{6\left(\frac{D_{fiber}}{2} + t_a\right)} \tag{47}$$

where t_b is the thickness of the aerogel blanket. Since the deformation of one layer equals the deformation of one unit cell, finally, the total deformation can be reported as:

$$\delta_{tot} = N_{layers} \times \delta_{layer} \tag{48}$$

Therefore, by combining Eq. (42) to Eq.(48), the total deformation of an aerogel blanket can be obtained from a closed form analytical relationship shown in Eq.(49):

$$\delta_{tot} = \frac{4 t_b P_{tot} {l_f}^5}{9\left(D_f + 2t_a\right)\left(EI\right)_{fiber}} \tag{49}$$

Eq. (50) is a non-dimensionalized compact relationship between the compressive strain, *e*, and the mechanical load (stress), *γ*, presented as follows:

$$e = \gamma\left(\frac{4 {l_{fiber}}^5}{9\left(D_{fiber} + 2t_a\right)\left(EI\right)_{fiber}}\right) \tag{50}$$

Compressing aerogel blankets results in a change in its microstructure, thus the porosity varies with compression. Assuming that the volume of fibers and aerogel particles (solid volume) do not change at each loading step and only the pore volume decreases, the new porosity can be calculated using the new thickness of the sample. Therefore, the expected porosity can be defined based on the relation for a change in volume, where *M* is the compression factor (ratio of the uncompressed blanket thickness to the compressed thickness at each loading step; *i.e.*, $t_{b,initial}/t_{b,new}$ where $t_{b,initial}$ and $t_{b,new}$ are the initial and new thickness of

the aerogel blanket, respectively, and ε_b is the void fraction of the aerogel blanket material ($0<\varepsilon_b<1$).

$$\varepsilon_{b,new} = 1 - M\left(1 - \varepsilon_{b,initial}\right) \tag{51}$$

Using Eq.(51), the new porosity can be obtained after each load increment and thickness calculation. The algorithm for this porosity modification is presented in Figure 25.

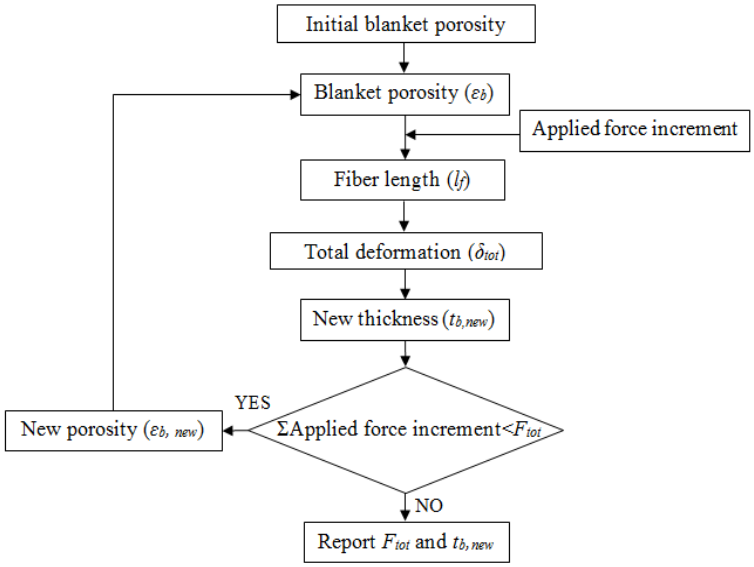

Figure 25. Porosity modification algorithm.

The mentioned algorithm can be expressed in a compact relationship as follows to calculate the blanket deformation directly at each loading step, Eq.(52):

$$\lim_{n\to\infty}\delta_i = t_{b,i-1}\frac{P_{tot,i}}{n}\frac{2l_{fiber_{i-1}}^5}{9(EI)_{fiber}\left(\frac{D_{fiber}}{2}+t_a\right)}, \qquad i=1,\ldots,n \tag{52}$$

where $l_{fiber,i-1}$ has to be calculated from Eq.(53):

$$l_{fiber,i-1} = \frac{\pi D_{fiber}^2 + 4\pi(1-\varepsilon_a)(D_{fiber}t_a + t_a^2) + \sqrt{16\pi}\sqrt{3072(1-\varepsilon_a)\left[\frac{t_{b,initial}}{t_{b,i-1}}(1-\varepsilon_{b,initial})\right]\left(\frac{D_{fiber}}{2}+t_a\right)^4 + \pi\left(\frac{1}{4}D_{fiber}^2 + (1-\varepsilon_a)(D_{fiber}t_a + t_a^2)\right)^2}}{32\left(\frac{D_{fiber}}{2}+t_a\right)\left[\frac{t_{b,initial}}{t_{b,i-1}}(1-\varepsilon_{b,initial})\right]} \tag{53}$$

3.2. Experimental Study

In this study, the same samples mentioned in Table 2-2 are used to perform compression tests and cycling study using HFM and TMA. Another feature of HFM is regulating the compression precisely and measuring the sample thickness with controlled loads up to 21 kPa.

A TMA (Q400EM, TA Instruments) with a macro-expansion probe with a 6.07 mm diameter contact area was used to compress 7 mm × 7 mm insulation samples. Two samples of each of type of the aerogel blanket insulations were tested with a linear ramp force up to 0.4 N in a dry nitrogen environment at room temperature. A schematic of the TMA instrument is shown in Figure 26. TMA measures sample displacement at various temperatures, times, and applied forces and its resolution for displacement is less than 0.5 nm.

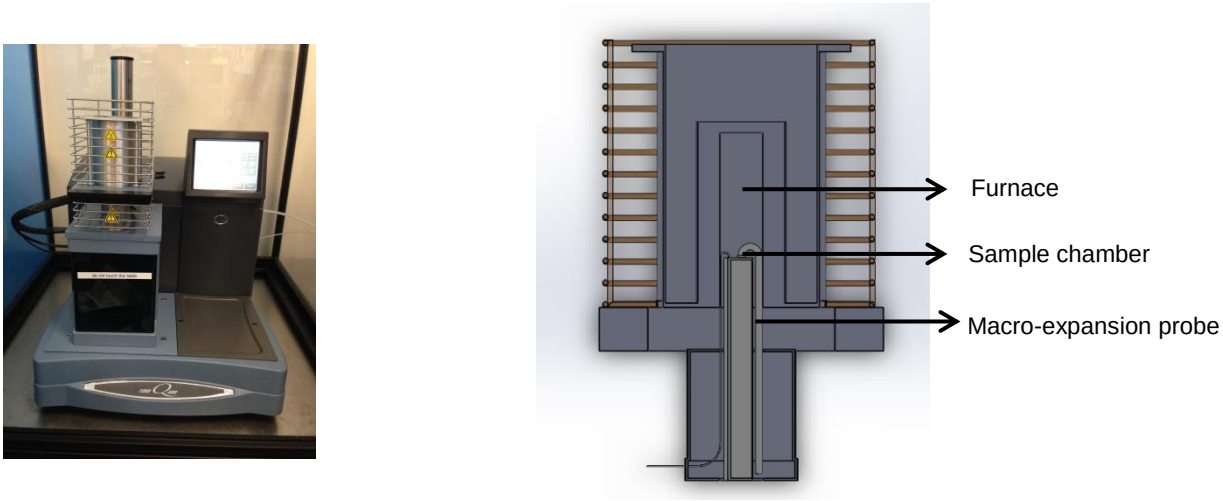

(a) (b)

Figure 26. (a) TMA device, and (b) its schematic [102]

The changes in the morphology of the material under compression were evaluated by Nano- SEM. For this purpose, samples were pressed up to a predetermined load at room temperature, which was the maximum load applied on the samples using HFM and TMA, and the images were taken under no-load and compressed conditions. In these images, the compressed material does not show any noticeable difference compared to its original state, Figure 27.

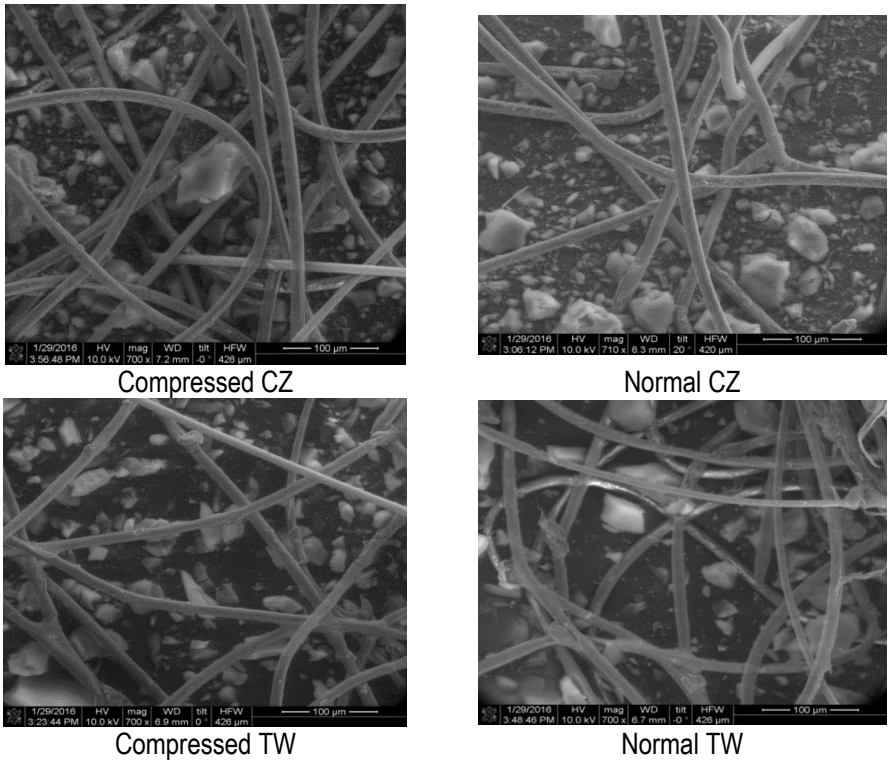

Figure 27. Microstructure of aerogel blanket samples; at no-load and compressed conditions.

3.3. Results and Discussion

In section 3.1, a nonlinear model is developed to predict the deformation of aerogel blanket samples as a function of stress applied on them. The parameters used in the analytical model are presented in Table 3-1.

Table 3-1. Constant parameters used in the compression analytical model.

Sample	Thickness	Fiber poison ratio	particle poison ratio [103]	Fiber modulus of elasticity	Particle modulus of elasticity [103]
CZ	10 mm	0.23 [104]	0.24	85 Gpa [104]	3 Mpa
	5 mm				
TW	8 mm	0.23 [105]	0.24	3.5 Gpa [105]	3 Mpa
	5 mm				

Figure 28 to Figure 31 present the results of the experiments performed by HFM and TMA and comparison to the developed model. The results of the proposed approach agreed well with the experimental data with low relative difference (maximum 10%) and show that

compression had minimal effect on the aerogel blanket insulation materials compared to the conventional insulation materials, *e.g.*, cellulose, rock wool, and fiberglass. In Ref. [57], large strain was measured under relatively low load. The authors reported 40% strain in fiberglass, 26% strain in rock wool, and 20% strain in cellulosic insulation material, after applying maximum of 0.14 kPa on the samples with initial thickness of 30 cm.

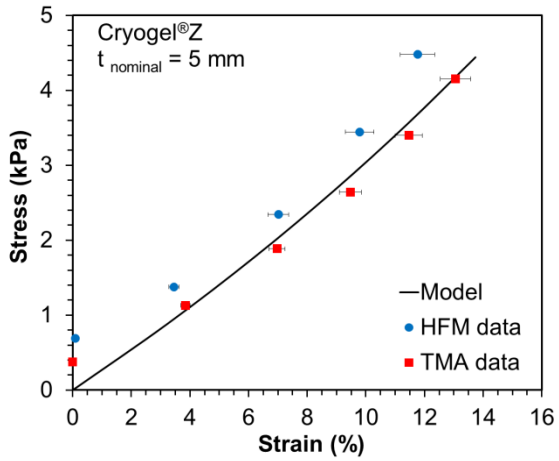

Figure 28. Stress-strain data and modeling result for CZ with 5 mm nominal thickness.

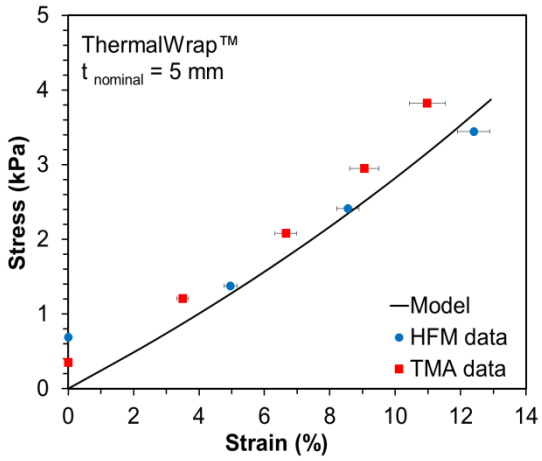

Figure 29. Stress-strain data and modeling result for TW with 5 mm nominal thickness.

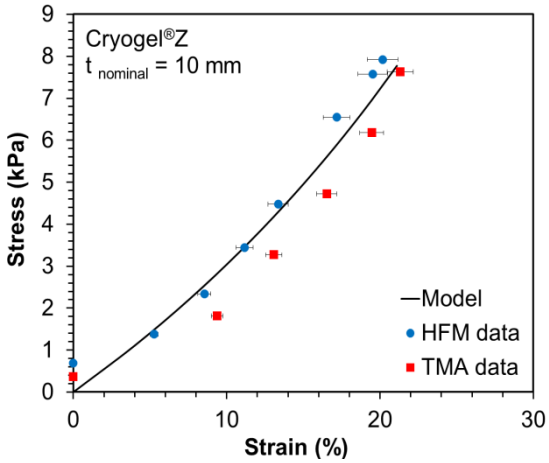

Figure 30. Sstress-strain data and modeling result for CZ with 10 mm nominal thickness.

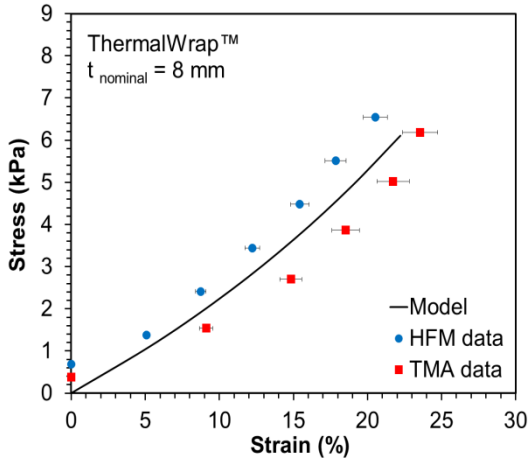

Figure 31. Stress-strain data and modeling result for TW with 5 mm nominal thickness.

Additionally, the effects of loading history on strain of the available samples were investigated. Presented in Figure 32, the changes to the materials under repeated loading cycles between 0.7 to 2 kPa for thinner samples and 0.7 to 5 kPa for thicker ones were subtle, and the responses of the materials to compression became stable after ~10 cycles of

mechanical deformation. Hysteresis in the HFM loading-unloading cycles indicated that plastic deformation occurred. This was attributed to the inelastic nature of aerogel blankets. Applying 20 compression-decompression cycles decreased the thickness of 10 mm CZ by 6% and the thickness of 8 mm TW by 3.5%. For the 5 mm samples, a thickness reduction of 2% for CZ and 1.5% for TW were observed, respectively.

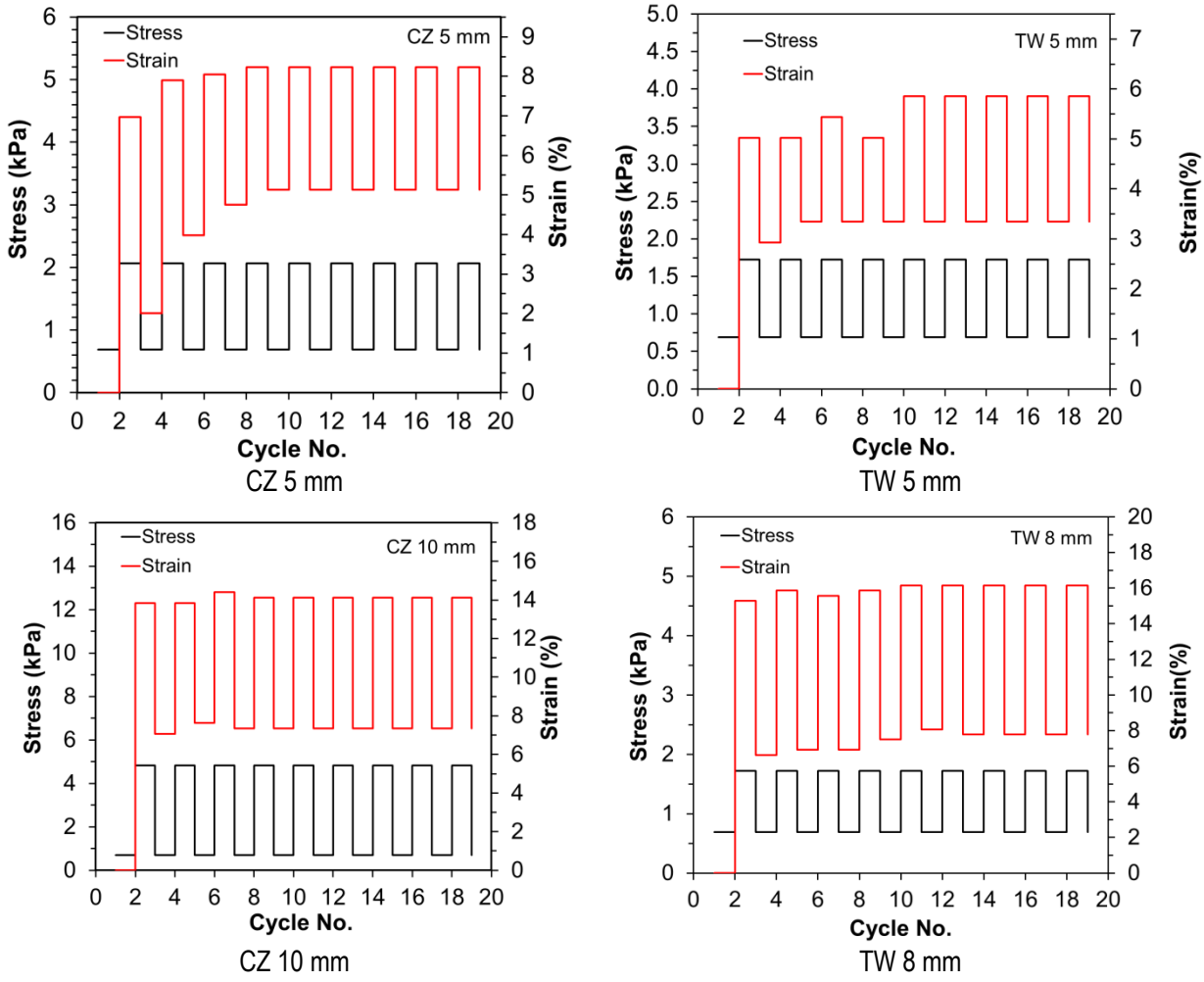

Figure 32. Cycle test for load range of 0.7-2 kPa for thinner samples and 0.7-5 kPa for thicker ones

Chapter 4.

Aerogel Blanket Combined Thermal and Mechanical Deformation Analysis

Aerogel blankets can be used in a variety of enclosures and are greatly relied upon for their very low thermal conductivity. Normally, if the material gets compressed, the thermal resistance will decrease. Hence, it is essential to consider similar conditions for the compaction of the sample in modeling the thermal properties.

4.1. The Present Model

The relationship for predicting the deformation of aerogel blanket samples under uniaxial compression from section 3.1 can be extended to predict the thermal resistance of the samples at various compressions. The relationship between the thermal resistance, thickness, and effective thermal conductivity is as follows:

$$R = \frac{t_{b,i}}{k_{eff} \cdot A_{sample}} \qquad i = 1, 2 \tag{54}$$

In Eq. (54), the thickness can be calculated having the deformation and new porosity at each loading (Eq.(52)) and the thermal conductivity as a function of temperature and new porosity using Eq.(8), following section 2.1.12.1.4, at dry and humid conditions.

4.2. Experimental Study

The thermal resistance of typical insulation materials decreases with compression. Therefore, it is essential to control sample compression during thermo-physical property testing. In this section, HFM was employed to measure the thermal conductivity (k-value) and thermal resistance (R-value) of aerogel blankets over a range of compression. The maximum load that HFM can apply on samples depends on two factors: 1) the compression load cannot be greater than 21 kPa; 2) the combined thickness of the specimen, the heat flux transducer, and any damping material, which in total equals the distance between the cold and hot plates, must be controlled to be large enough in order to minimize the effect of edge losses on the measurement

of heat flux [18]. In this study, insulation samples (30.5 cm × 30.5 cm) were tested between two heat flux sensors under a specific temperature gradient, applied by a hot plate and cold plate. Each specimen was tested under increasing loads to the minimum allowed sample thickness. The total thermal resistance was calculated from the equilibrium temperature difference across the sample and the known heat flux applied to the sample. Further details of the apparatus and the methodology used in the thermal resistance measurements can be found in ASTM C518 [99].

4.3. Results and Discussion

Series of measurements were performed using HFM to study the variation of samples thermal resistances as a function of their thicknesses as shown in Figure 33. Linear relationship between normalized thermal resistance and thickness shows that the thermal conductivity almost remains constant during compression, considering the fact that the area is kept constant for all the experiments.

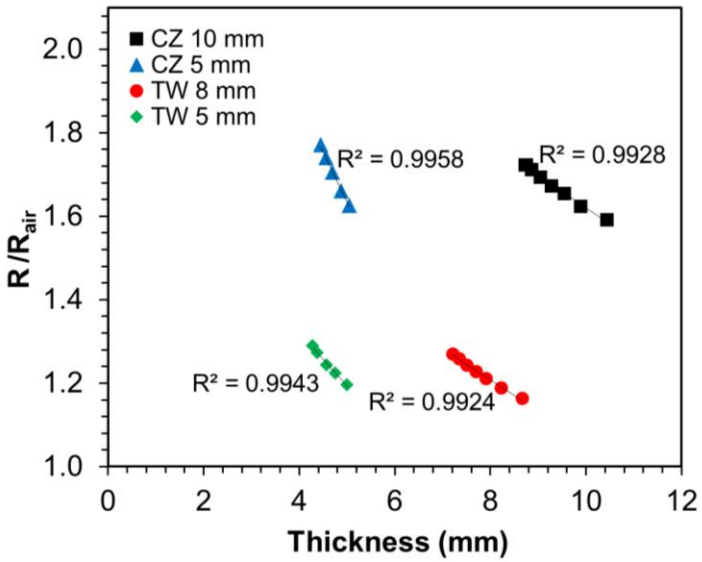

Figure 33. Total resistance variation as a function of thickness.

Figure 34 and Figure 35 demonstrate the variation of resistance as a function of compressive load for four different samples. The error bars represent the standard deviation of the measurements. The R-values were obtained at reduced thicknesses as a function of compression without removing the insulation specimen from the HFM. Results show that when the compression load was increased from 0.7 to 4.5 kPa, the resistance decreased 8.5% for CZ

and 9% for TW for samples with 5 mm thickness. These values for samples with higher thicknesses were 10% and 8.5% for CZ and TW, respectively. Hence, it can be concluded that resistance reduction in aerogel blanket insulation can be as high as 10% under ~7 kPa compression, which is only due to mechanical deformation, *i.e.*, thickness reduction. The resistance reduction from full thickness condition of 30 cm for rock wool, cellulose, and fiberglass after applying just about 0.14 kPa load were shown to be 20%, 23%, and 20%, respectively [57], which is much greater than the thermal resistance loss that occurs for aerogel blanket under similar condition. Hence, aerogel blankets are remarkably more efficient thermal insulation materials in terms of thermal performance, space occupation (considering the required thickness of conventional insulations for having almost the same thermal resistance as aerogel blankets), deformation and thermal resistance loss under compression.

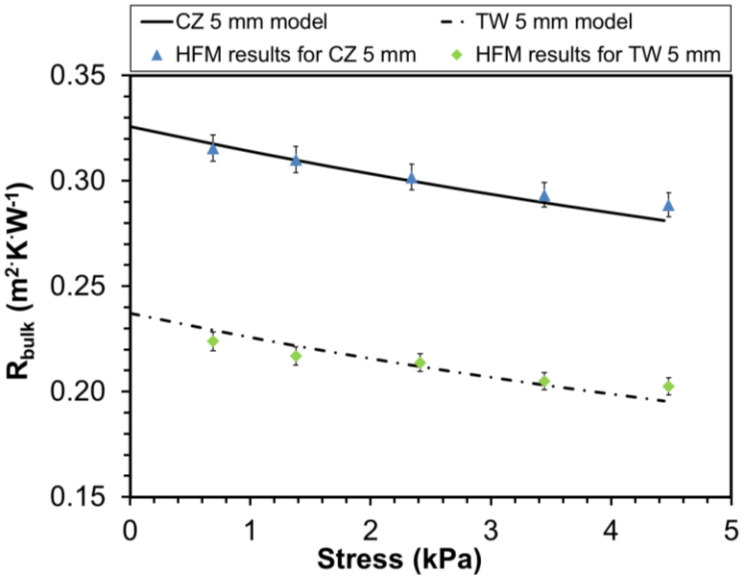

Figure 34. Resistance variation of CZ of 5 mm nominal thickness and TW of 5 mm nominal thickness at various compressive loads.

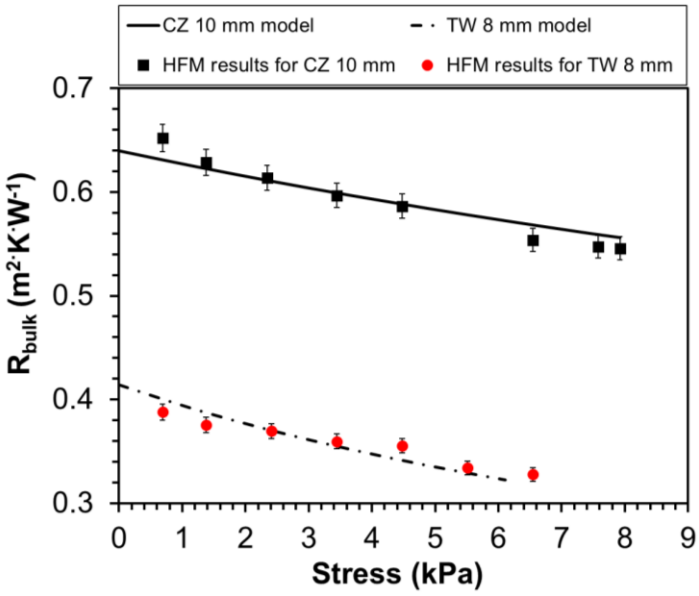

Figure 35. Resistance variation of CZ of 10 mm nominal thickness and TW of 8 mm nominal thickness at various compressive loads.

Chapter 5.

Summary and Future Work

5.1. Summary of Thesis

In this thesis, a comprehensive experimental and theoretical study of the thermal and mechanical performance of aerogel blankets were performed considering the effect of temperature and moisture content at transient and steady-state conditions as well as deformation under uniaxial compression. Although each effect was modeled separately, they are all based on mutual assumptions and followed the same method, which is unit cell approach. Defining identical unit cells gave us the option of connecting them together in order to thoroughly analyse a material by one analytical modeling package. In other words, having specifications of an aerogel blanket such as fiber diameter, fiber thermal conductivity, porosity, and average pore size as input of the model, one can get R-value of the sample under defined T, RH and mechanical pressure. The followings summarize the research and findings of this thesis:

- Material characterizations such as porosity, FTIR measurements, SEM, and Nano SEM imaging were performed on two types of commercially available aerogel blankets.

- An analytical model was developed for predicting the effective thermal conductivity as a function of temperature, which accounted for solid and gas conduction as well as radiation, and was validated with experimental data from heat flow meter (HFM) under dry conditions (RH=0%).

- Temperature study of aerogel blankets showed that their effective thermal conductivity is lower than that of many other conventional types of insulation materials in a wide range of temperatures. Also, increasing temperature results in increasing the effective thermal conductivity.

- Moisture build up in two aerogel blanket samples were measured as a function of RH and temperature. The results showed that moisture content increased at higher RH and lower temperature.

- A set up of transient plane source (TPS) and humidifier assembly was designed and developed to measure the thermal conductivity under varying humidity conditions.

- Experimental study of aerogel blankets at steady-state condition using TPS-humidifier assembly revealed that the effective thermal conductivity of the investigated samples increased by increasing RH. This trend can be explained by considering the higher thermal conductivity of the inbuilt moisture compared to dry air as the filling fluid inside the pores.

- Thermal conductivity cyclic tests showed that it took approximately six cycles, of 5 hours rest time, till the effective thermal conductivity reaches its maximum, which means the material was holding all the moisture that it could.

- A new moisture diffusion model was introduced using the concept of RC circuit, based on the analogy between electrical and mass transfer phenomena. This model was integrated to the analytical model of thermal conductivity as a function of temperature to include the effect of moisture diffusion in that model.

- An extended version of the T and RH unit cell was used to model the effect of deformation on R-value of aerogel blankets.

- The analytically predicted deformation of aerogel blanket under compression matched well with the experimental results from tests performed with the HFM and thermomechanical analyzer.

- Compression modeling and tests results showed small variation of R-value by increasing mechanical load on the materials. It indicated that aerogel blankets remain remarkably effective even under compression.

5.2. Future Work

The following research directions can be considered as the continuation of this study:

- The diffusion coefficient was investigated for just one aerogel blanket sample (CZ) due to time limitations. The long-term measurements can also be done on other samples to find their diffusion coefficient and time constant.
- Experimental procedures can be developed to measure the moisture diffusion into aerogel blankets, to obtain more reliable data for diffusion coefficient.
- The analytical model can be upgraded to a more advanced model by adding pore size distribution and water droplet distribution inside the pores.
- Condensation can be studied separately in the humidity model to include both concentration and temperature gradient effects on moisture diffusion.
- Long-term measurements of the effect of mechanical loading on the samples can be done (creep tests) to study the degradation process of the material under compression.
- Effect of compression under different humidity and temperature conditions would be a nice addition to this study.
- Using the developed analytical model, optimization study can be done to design more efficient and cost-effective aerogel blankets.

References

[1] International Energy Agency, “Technology Roadmap,” *Oecd*, p. 68, 2013.

[2] L. Pérez-Lombard, J. Ortiz, and C. Pout, “A review on buildings energy consumption information,” *Energy Build.*, vol. 40, no. 3, pp. 394–398, 2008.

[3] Natural Resources Canada (NRC), “Energy efficiency trends in Canada 1990 to 2009,” 2011.

[4] Statistics Canada, “Households and the environment: energy Use,” Ottawa, 2011.

[5] International Energy Agency, “Transition to Sustainable Buildings,” 2013.

[6] O. C. Perez, “The behavior of aerogel blankets as insulation material in external walls at high temperatures,” Chalmers university of technology, 2012.

[7] Energy Information Administration, *International Energy Outlook*, vol. 484, no. June. 2006.

[8] L. F. Cabeza, A. Castell, M. Medrano, I. Martorell, G. Pérez, and I. Fernández, “Experimental study on the performance of insulation materials in Mediterranean construction,” *Energy Build.*, vol. 42, no. 5, pp. 630–636, 2010.

[9] A. A. Abdou and I. M. Budaiwi, “Comparison of Thermal Conductivity Measurements of Building Insulation Materials under Various Operating Temperatures,” *J. Build. Phys.*, vol. 29, no. 2, pp. 171–184, 2005.

[10] B.-M. Zhang, S.-Y. Zhao, and X.-D. He, “Experimental and theoretical studies on high-temperature thermal properties of fibrous insulation,” *J. Quant. Spectrosc. Radiat. Transf.*, vol. 109, no. 7, pp. 1309–1324, 2008.

[11] A.-L. Pasanen, S. Rautiala, J. P. Kasanen, P. Raunio, J. Rantamäki, and P. Kalliokoski, “The relationship between measured moisture conditions and fungal concentrations in water-damaged building materials.,” *Indoor Air*, vol. 10, no. 2, pp. 111–120, 2000.

[12] K. Huttunen, H. Rintala, M. R. Hirvonen, A. Vepsäläinen, A. Hyvärinen, T. Meklin, M. Toivola, and A. Nevalainen, “Indoor air particles and bioaerosols before and after renovation of moisture-damaged buildings: The effect on biological activity and microbial flora,” *Environ. Res.*, vol. 107, no. 3, pp. 291–298, 2008.

[13] J. Lstiburek, N. Yost, and T. Brennan, “Mold: Causes, Health Effects and Clean-Up,” 2002.

[14] J. Fan and X. Wen, “Modeling heat and moisture transfer through fibrous insulation with phase change and mobile condensates,” *Int. J. Heat Mass Transf.*, vol. 45, no. 19, pp. 4045–4055, Sep. 2002.

[15] J. Fan and X. X. Wen, “An improved model of heat and moisture transfer with phase change and mobile condensates in fibrous insulation and comparison with experimental results,” *Int. J. Heat Mass Transf.*, vol. 47, no. 10–11, pp. 2343–2352, May 2004.

[16] F. Björk and T. Enochsson, “Properties of thermal insulation materials during extreme environment changes,” *Constr. Build. Mater.*, vol. 23, no. 6, pp. 2189–2195, 2009.

[17] “Thermal insulation products for buildings — Factory made mineral wool (MW) products — Specification,” Wien, 2009.

[18] T. Vrana, “Impact of Moisture on Long Therm Performance of Insulating Products,” KTH – The Royal Institute of Technology, 2007.

[19] H. Maleki, L. Durães, and A. Portugal, “An overview on silica aerogels synthesis and different mechanical reinforcing strategies,” *J. Non. Cryst. Solids*, vol. 385, pp. 55–74, 2014.

[20] G. W. Brinker, C. J.; Scherer, *Sol-Gel Science*. 1990.

[21] J. Ryu, “Flexible aerogel superinsulation and its manufacture,” 6,068,882.

[22] G. Wei, X. Zhang, and F. Yu, “Effective thermal conductivity analysis of xonotlite-aerogel composite insulation material,” *J. Therm. Sci.*, vol. 18, no. 2, pp. 142–149,

May 2009.

[23] J. M. S. F. Rouanet, R. K. Massey, “Aerogel containing blanket,” 7635411 B2, 2009.

[24] “https://www.alibaba.com/product-detail/Aerogel-Powder-Beads_111240339.html.” .

[25] “http://www.tradekorea.com/product/detail/P485142/Aerogel-blanket.html.” .

[26] R. and A.-C. E. American Society of Heating, *ASHRAE Handbook: Fundamentals*, SI Edition. Atlanta, Ga: American Society of Heating Refrigerating and Air-Conditionin, 2005.

[27] D. P. Rizzetta, M. R. Visbal, M. J. Stanek, G. R. Cunnington, and S. C. Lee, “Radiative properties of fibrous insulations - Theory versus experiment,” *J. Thermophys. Heat Transf.*, vol. 10, no. 3, pp. 460–466, 1996.

[28] S.-C. Lee and G. R. Cunnington, “Conduction and Radiation Heat Transfer in High-Porosity Fiber Thermal Insulation,” *J. Thermophys. Heat Transf.*, vol. 14, no. 2, pp. 121–136, Apr. 2000.

[29] Kyung Wha Oh and S. H. K. Kim, “Ultra-porous flexible PET/Aerogel blanket for sound absorption and thermal insulation,” *Fibers Polym.*, vol. 10, no. 5, pp. 731–737, Nov. 2009.

[30] J. Wang, J. Kuhn, and X. Lu, “Monolithic silica aerogel insulation doped with TiO2 powder and ceramic fibers,” *J. Non. Cryst. Solids*, vol. 186, no. 95, pp. 296–300, 1995.

[31] G. Wei, Y. Liu, X. Zhang, F. Yu, and X. Du, “Thermal conductivities study on silica aerogel and its composite insulation materials,” *Int. J. Heat Mass Transf.*, vol. 54, no. 11–12, pp. 2355–2366, 2011.

[32] G. Lu, X. D. Wang, Y. Y. Duan, and X. W. Li, “Effects of non-ideal structures and high temperatures on the insulation properties of aerogel-based composite materials,” *J. Non. Cryst. Solids*, vol. 357, no. 22–23, pp. 3822–3829, 2011.

[33] G. Wei, Y. Liu, X. Zhang, F. Yu, and X. Du, “Thermal conductivities study on silica aerogel and its composite insulation materials,” *Int. J. Heat Mass Transf.*, vol. 54, no. 11–12, pp. 2355–2366, May 2011.

[34] R. Coquard, D. Baillis, V. Grigorova, F. Enguehard, D. Quenard, and P. Levitz, “Modelling of the conductive heat transfer through nano-structured porous silica materials,” *J. Non. Cryst. Solids*, vol. 363, pp. 103–115, Mar. 2013.

[35] J. B. Alvey, “performance of aerogel composite and foam insulations,” University of Illinois at Urbana-Champaign, 2014.

[36] N. Gupta and W. Ricci, “Processing and compressive properties of aerogel/epoxy composites,” *J. Mater. Process. Technol.*, vol. 198, pp. 178–182, 2008.

[37] T. Xie, Y.-L. He, and Z.-J. Hu, “Theoretical study on thermal conductivities of silica aerogel composite insulating material,” *Int. J. Heat Mass Transf.*, vol. 58, no. 1–2, pp. 540–552, Mar. 2013.

[38] J.-J. Zhao, Y.-Y. Duan, X.-D. Wang, and B.-X. Wang, “Radiative properties and heat transfer characteristics of fiber-loaded silica aerogel composites for thermal insulation,” *Int. J. Heat Mass Transf.*, vol. 55, no. 19–20, pp. 5196–5204, Sep. 2012.

[39] B. T. Chaddock, J. B., “Heat and mass transfer in building materials and structures,” in *21st symposium of the International Centre for Heat and Mass Transfer (ICHMT)*, 1991.

[40] J. C. Alvarez, “Evaluation of Moisture Diffusion Theories in Porous Materials,” Virginia Polytechnic Institute and State University In, 1998.

[41] E. S. Saltzman, D. B. King, K. Holmen, and C. Leck, “Experimental Determination of the Diffusion Coefficient of Water in Transformer Solid Insulation,” *J. Geophys. Res.*, vol. 98, no. C9, p. 16481, 1993.

[42] D. F. García, B. García, and J. C. Burgos, “Determination of moisture diffusion coefficient for oil-impregnated Kraft-paper insulation,” *Int. J. Electr. Power Energy Syst.*, vol. 53, no. 1, pp. 279–286, 2013.

[43] D. G. Stephenson, “Thermal diffusion of water vapour through glass fibre insulation,” in *e-Sim 2004 Conference*, 2004, pp. 1–6.

[44] Z. Pavlík, L. Fiala, E. Vejmelková, and R. Černý, “Application of effective media theory for determination of thermal properties of hollow bricks as a function of moisture content,” *Int. J. Thermophys.*, vol. 34, no. 5, pp. 894–908, 2013.

[45] Z. Pavlík, E. Vejmelková, L. Fiala, and R. Černý, “Effect of moisture on thermal conductivity of lime-based composites,” *Int. J. Thermophys.*, vol. 30, no. 6, pp. 1999–2014, 2009.

[46] E. Vejmelková, M. Keppert, P. Rovnaníková, Z. Keršner, and R. Černý, “Application of burnt clay shale as pozzolan addition to lime mortar,” *Cem. Concr. Compos.*, vol. 34, no. 4, pp. 486–492, 2012.

[47] A. Karamanos, S. Hadiarakou, and A. M. Papadopoulos, “The impact of temperature and moisture on the thermal performance of stone wool,” *Energy Build.*, vol. 40, no. 8, pp. 1402–1411, 2008.

[48] A. Abdou and I. Budaiwi, “The variation of thermal conductivity of fibrous insulation materials under different levels of moisture content,” *Constr. Build. Mater.*, vol. 43, pp. 533–544, 2013.

[49] M. Jerman and R. Černý, “Effect of moisture content on heat and moisture transport and storage properties of thermal insulation materials,” *Energy Build.*, vol. 53, pp. 39–46, 2012.

[50] F. Ochs, W. Heidemann, and H. Müller-Steinhagen, “Effective thermal conductivity of moistened insulation materials as a function of temperature,” *Int. J. Heat Mass Transf.*, vol. 51, no. 3–4, pp. 539–552, 2008.

[51] O. Krischer and W. Kast, “Die wissenschaftlichen Grundlagen der Trocknungstechnik,” *Springer*, 1992.

[52] Á. Lakatos, “Investigation of the moisture induced degradation of the thermal properties of aerogel blankets: Measurements, calculations, simulations,” *Energy Build.*, vol. 139, pp. 506–516, 2017.

[53] R. Galliano, K. Ghazi Wakili, T. Stahl, B. Binder, and B. Daniotti, “Performance evaluation of aerogel-based and perlite-based prototyped insulations for internal thermal retrofitting: HMT model validation by monitoring at demo scale,” *Energy Build.*, vol. 126, pp. 275–286, 2016.

[54] T. Stahl, S. Brunner, M. Zimmermann, and K. Ghazi Wakili, “Thermo-hygric properties of a newly developed aerogel based insulation rendering for both exterior and interior applications,” *Energy Build.*, vol. 44, pp. 114–117, Jan. 2012.

[55] T. Ihara, B. P. Jelle, T. Gao, and A. Gustavsen, “Aerogel granule aging driven by moisture and solar radiation,” *Energy Build.*, vol. 103, pp. 238–248, 2015.

[56] K. Ghazi Wakili, T. Stahl, E. Heiduk, M. Schuss, R. Vonbank, U. Pont, C. Sustr, D. Wolosiuk, and A. Mahdavi, “High performance aerogel containing plaster for historic buildings with structured façades,” *Energy Procedia*, vol. 78, no. 0, pp. 949–954, 2015.

[57] D. W. Yarbrough and J. ti. Wright, “Reduction in the thermal resistance of loose fill insulation and fiberglass batts due to compression,” Cookeville, Tennessee, 1981.

[58] R. D. Adams and J. G. Hust, “A round robin on apparent thermal conductivity of several loose-fill insulations,” *Insul. Mater. Test. Appl. ASTM STP 1030*, pp. 263–289, 1990.

[59] R. S. Graves and D. W. Yarbrough, “The effect of compression on the material R - Value of fiberglass batt Insulation,” *J. Therm. Insul.*, vol. 15, pp. 248–260, 1992.

[60] J. G. Symons and V. Clarke, R. E. ClarkePeirce, “The thermal performance of several Australian fibrous insulating materials,” *Therm. Insul. bldg. Envs.*, vol. 19, no. July, pp. 72–88, 1995.

[61] M. Kolich, P. Hoke, D. Dooge, M. Doroudian, E. Litovsky, and J. Kleiman, “Influence of temperature and mechanical compression on thermophysical properties of car interior foam plastics insulation,” *J. Elastomers Plast.*, vol. 46, no. 2, pp. 132–143, 2014.

[62] E. Cuce, P. M. Cuce, C. J. Wood, and S. B. Riffat, “Optimizing insulation

thickness and analysing environmental impacts of aerogel-based thermal superinsulation in buildings," *Energy Build.*, vol. 77, pp. 28–39, 2014.

[63] E. R. Bardy, J. C. Mollendorf, and D. R. Pendergast, "Thermal conductivity and compressive strain of aerogel insulation blankets under applied hydrostatic pressure," *J. Heat Transfer*, vol. 129, no. 2, p. 232, 2007.

[64] D. Shi, Y. Sun, J. Feng, X. Yang, S. Han, C. Mi, Y. Jiang, and H. Qi, "Experimental investigation on high temperature anisotropic compression properties of ceramic-fiber-reinforced SiO2 aerogel," *Mater. Sci. Eng. A*, vol. 585, pp. 25–31, 2013.

[65] H. Wu, Y. Liao, Y. Ding, H. Wang, C. Peng, and S. Yin, "Engineering thermal and mechanical properties of multilayer aligned fiber-reinforced aerogel composites," *Heat Transf. Eng.*, vol. 35, no. 11–12, pp. 1061–1070, 2014.

[66] a Tamayol and M. Bahrami, "Numerical investigation of flow in fibrous porous media," no. September, pp. 21–26, 2008.

[67] a. Tamayol, K. W. Wong, and M. Bahrami, "Effects of microstructure on flow properties of fibrous porous media at moderate Reynolds number," *Phys. Rev. E*, vol. 85, no. January 2011, pp. 1–7, 2012.

[68] E. Sadeghi, M. Bahrami, and N. Djilali, "Analytic determination of the effective thermal conductivity of PEM fuel cell gas diffusion layers," *J. Power Sources*, vol. 179, no. 1, pp. 200–208, Apr. 2008.

[69] A. Ahern, G. Verbist, D. Weaire, R. Phelan, and H. Fleurent, "The conductivity of foams: a generalisation of the electrical to the thermal case," *Colloids Surfaces A Physicochem. Eng. Asp.*, vol. 263, no. 1–3, pp. 275–279, 2005.

[70] G. Wei, Y. Liu, X. Zhang, F. Yu, and X. Du, "Thermal conductivities study on silica aerogel and its composite insulation materials," *Int. J. Heat Mass Transf.*, vol. 54, no. 11–12, pp. 2355–2366, May 2011.

[71] J. H. Vansant, *Conduction heat transfer solutions*, no. March. 1980.

[72] L. Huang, “Feasibility study of using silica aerogel as insulation for buildings,” KTH University, 2012.

[73] G. B. a. Carotenuto, “the Effective Thermal Conductivity of Packed Beds of Spheres for a Finite Contact Area,” *Numer. Heat Transf. Part A Appl.*, vol. 37, no. 4, pp. 343–357, Mar. 2000.

[74] G. Buonanno, a. Carotenuto, G. Giovinco, and N. Massarotti, “Experimental and Theoretical Modeling of the Effective Thermal Conductivity of Rough Steel Spheroid Packed Beds,” *J. Heat Transfer*, vol. 125, no. 4, p. 693, 2003.

[75] N. M. G. Buonanno, A. Carotenuto, G. Giovinco and Sarotti, “Effective thermal conductivity of rough spheres packed beds,” in *Proceedings of HT2003, ASME Heat Transfer Conference*, 2003.

[76] Y. Ogniewicz and M. M. Yovanovich, “Effective conductivity of regularly packed spheres: basic cell model with constriction,” in *L.S. Fletcher (Ed.), Heat Transfer and Thermal Control Systems*, 1987.

[77] P. J. Turyk and M. M. Yovanovich, “Modified effective conductivity models for basic cells of simple cubic packed beds,” in *Proc. 23rd National Heat Transfer Conference*, 1985, pp. 9–19.

[78] M. Bahrami, M. M. Yovanovich, and J. R. Culham, “Effective thermal conductivity of rough spherical packed beds,” *Int. J. Heat Mass Transf.*, vol. 49, no. 19–20, pp. 3691–3701, Sep. 2006.

[79] G. Wei, Y. Liu, X. Du, and X. Zhang, “Gaseous Conductivity Study on Silica Aerogel and Its Composite Insulation Materials,” *J. Heat Transfer*, vol. 134, no. 4, p. 41301, 2012.

[80] C. T. HSU, P. CHENG, and K. W. Wong, “Modified Zehner-Schlunder models for stagnant thermal conductivity of porous media,” *Heat mass Transf.*, vol. 31, no. 17, pp. 2751–2759, 1994.

[81] J.-S. Kwon, C. H. Jang, H. Jung, and T.-H. Song, “Effective thermal conductivity of various filling materials for vacuum insulation panels,” *Int. J. Heat Mass Transf.*,

vol. 52, no. 23–24, pp. 5525–5532, Nov. 2009.

[82] S. Jennings, “The Mean Free Path in Air,” *J. Aerosol Sci.*, vol. 19, no. 2, pp. 159–166, 1988.

[83] P. Noiying, M. Hinaje, P. Thounthong, S. Raël, and B. Davat, “Using electrical analogy to describe mass and charge transport in PEM fuel cell,” *Renew. Energy*, vol. 44, pp. 128–140, 2012.

[84] J. N. Davidson, D. A. Stone, M. P. Foster, and C. R. Gould, “Prediction of device temperatures in an electric vehicle battery charger system by analysis of device thermal cross-coupling,” *2013 15th Eur. Conf. Power Electron. Appl. EPE 2013*, 2013.

[85] J. N. Davidson, D. A. Stone, and M. P. Foster, “Required Cauer network order for modelling of thermal transfer impedance,” *Electron. Lett.*, vol. 50, no. 4, pp. 1–2, 2014.

[86] K. Murthy and R. Bedford, “Transformation between Foster and Cauer equivalent networks,” *IEEE Trans. Circuits Syst.*, vol. 25, no. 4, pp. 238–239, 1978.

[87] A. Gholami, M. Ahmadi, and M. Bahrami, “A New Analytical Approach for Dynamic Modeling of Passive Multicomponent Cooling Systems,” *J. Electron. Packag.*, vol. 136, no. 3, p. 31010, 2014.

[88] M. Becherif, D. Hissel, S. Gaagat, and M. Wack, “Electrical equivalent model of a proton exchange membrane fuel cell with experimental validation,” *Renew. Energy*, vol. 36, no. 10, pp. 2582–2588, 2011.

[89] A. Hernandez, D. Hissel, and R. Outbib, “Modeling and fault diagnosis of a polymer electrolyte fuel cell using electrical equivalent analysis,” *IEEE Trans. Energy Convers.*, vol. 25, no. 1, pp. 148–160, 2010.

[90] P. R. Pathapati, X. Xue, and J. Tang, “A new dynamic model for predicting transient phenomena in a PEM fuel cell system,” *Renew. Energy*, vol. 30, no. 1, pp. 1–22, 2005.

[91] K. J. Runtz and M. D. Lyster, “Fuel cell equivalent circuit models for passive mode testing and dynamic mode design,” *Can. Conf. Electr. Comput. Eng.*, vol. 2005, no. May, pp. 794–797, 2005.

[92] A. S. Morris, *Measurement and instrumentation principles*, 3rd ed. Oxford: Butterworth-Heinemann, 2001.

[93] J. C. Maxwell, *A TREATISE ON ELECTRICITY AND MAGNETISM*, vol. 1, no. 9. Uonfron MACMILLAN AND CO., 1873.

[94] Á. Lakatos, “Moisture induced changes in the building physics parameters of insulation materials,” *Sci. Technol. Built Environ.*, vol. 22, no. 3, pp. 252–260, 2016.

[95] J. R. Siegel, Robert; Howell, *Thermal Radiation heat transfer*, 3rth ed. Washington, D.C.: Hemisphere publishing Corporation, 1993.

[96] M. U. Temp, “Cryogel ® Z data sheet.” .

[97] “Thermal wrap data sheet,” no. i. p. 2011, 2011.

[98] ISO22007-2, “Plastics-determination of thermal conductivity and thermal diffusivity-part 2: transient plane heat source (hot disc) method,” 2008.

[99] “ASTM C518-10, Standard test method for steady-state thermal transmission properties by means of the heat flow meter apparatus,” ASTM International, West Conshohocken, PA, 2010.

[100] “MATLAB.” .

[101] V. Norouzifard and M. Bahrami, “Deformation of PEM fuel cell gas diffusion layers under compressive loading: An analytical approach,” *J. Power Sources*, vol. 264, pp. 92–99, 2014.

[102] L. Waguespack, “Thermomechanical Analysis (TMA Q400EM/Q400 specifications),” 2013.

[103] “Marketech International Inc.” [Online]. Available: https://mkt-

intl.com/materials/aerogel/silica-aerogel/.

[104] “AZO Materials.” [Online]. Available: http://www.azom.com/properties.aspx?ArticleID=764.

[105] “The engineering toolbox.” [Online]. Available: http://www.engineeringtoolbox.com/young-modulus-d_417.html.

[106] D. Julve, J. Ramos, J. Pérez, and M. Menéndez, “Analysis of mercury porosimetry curves of precipitated silica, as an example of compressible porous solids,” *J. Non. Cryst. Solids*, vol. 357, no. 4, pp. 1319–1327, 2011.

[107] R. Pirard, S. Blacher, F. Brouers, and J. P. Pirard, “Interpretation of mercury porosimetry applied to aerogels,” *J. Mater. Res.*, vol. 10, no. 8, pp. 2114–2119, 1995.

Appendix A.

Pore size measurement

Mercury intrusion and nitrogen sorption are two techniques widely used to characterize the textural properties of mesoporous materials as data treatment methods [106]. The nitrogen adsorption-desorption isotherm analysis gives a distribution of specific surface area and pore volumes in a wide range of porosities from nanopores to mesopores of diameter smaller than 300 nm. Mercury intrusion porosimetry (MIP) gives information on the structure of the pores. The analysis of the distribution of the specific surface area and the specific pore volume in relation with the pore size from mercury porosimetry data is classically based on Washburn's equation. This equation has been derived on the assumption that the mercury intrudes the pore network [107].

Our results indicated that aerogel blankets have a pore diameter distribution that extends from the nanometer to micrometer range. The problem is that N_2 adsorption method captures the pore size range in which macro pores are not considered. On the other hand, although MIP captures pore size range of 3 nm to 0.1 mm, the very high pressure of mercury crushes the structure of the sample. In Figure 36 and Figure 37, the difference between MIP and N_2 adsorption porosimetry can be easily observed. According to our compression measurements using heat flow meter (HFM) (See Section 3.2), the maximum compressive load that, for example, 10 mm CZ was able to tolerate was less than 10 kPa (~1.5 psi). Knowing that the mercury intrusion starts from 1.5 psi pressure, it has been observed experimentally that the structure of the samples was damaged by the high pressure required to intrude small cells. That can be explained by the small value of the Young modulus and the ultimate compressive strength of aerogels. Consequently, Washburn's equation cannot be applied to aerogel blankets and the result of pore size distribution cannot be trusted. Hence, the images from scanning electron microscopy (SEM) were utilized to find the mean pore size of the samples statically, which was about 50 micrometer for CZ and 75 micrometer for TW. The drawback of this technique is related to the fact that it provides only a two-dimensional projection of a three-dimensional structure.

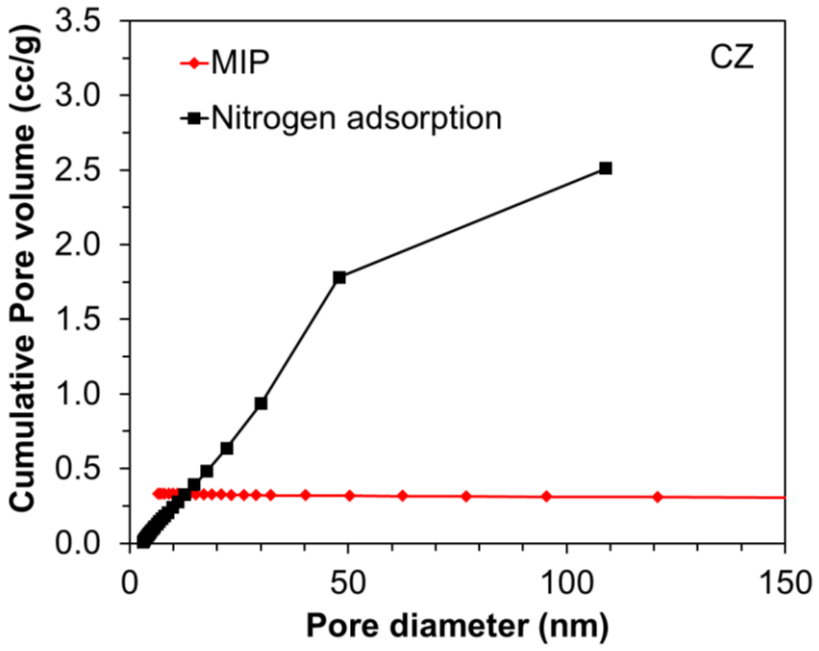

Figure 36. Cumulative pore volume of 10 mm thick CZ, measured by MIP and N_2 adsorption porosimetry

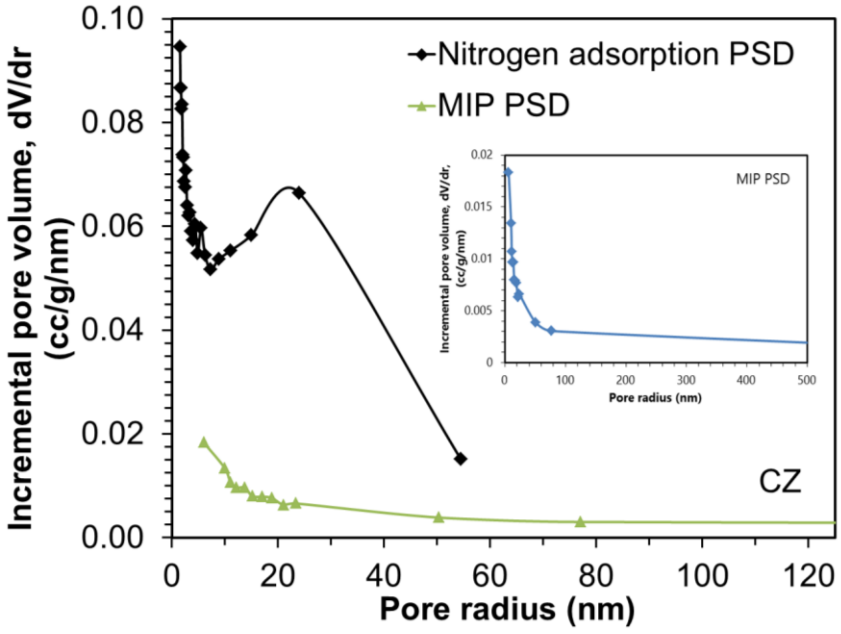

Figure 37. Incremental pore volume of 10 mm thick CZ, results of MIP and N_2 adsorption porosimetry.

Appendix B.

Experimental data

This appendix contains the experimental data of mechanical and thermal properties of the aerogel blanket samples collected in this research. The samples specifications are reported in Table B.1.

Table 0-1: Aerogel blanket samples specifications

Manufacturer Data [60, 61]

Sample	Provider	Thickness	Density*	Fiber composition	Powder material	Thermal* Conductivity
Cryogel® Z (CZ)	Aspen Aerogel	10 mm 5 mm	130 $kg \cdot m^{-3}$	Polyester/ fiber glass	Silica (SiO_2)	0.014 $W \cdot m^{-1} \cdot K^{-1}$
ThermalWrap™ (TW)	Cabot Corp.	8 mm 5 mm	70 $kg \cdot m^{-3}$	Polyester and polyethylene	Silica (SiO_2)	0.023 $W \cdot m^{-1} \cdot K^{-1}$

Measured Values

Sample	Particle diameter	Fiber Diameter	Porosity	Extinction coefficient
CZ	10 μm	20 μm	91%	4014 m^{-1}
TW	4 μm	7 μm	79%	3165 m^{-1}

*At room temperature

Cryogel® Z

Table 0-2: Measurements on 30.5 cm × 30.5 cm × 10 mm CZ using HFM (Netzsch HFM 436 Lambda) @ RH=0%, compressive load=0.5 Psi and temperature gradient= 40˚C following ASTM C518

T (°C)	k ($W \cdot m^{-1} \cdot K^{-1}$)
-20	0.0147
-10	0.0148
0	0.0151
10	0.0154
20	0.0154
30	0.0157
40	0.0159
50	0.0161
60	0.0164
70	0.0164
80	0.0165

Table 0-3: Measurements on 30.5 cm × 30.5 cm × 10 mm CZ using environmental chamber, ESPEC Platinous series EPX-4H and Ohaus AdventurerTM Balance following ISO 12571:2013 Standard

T (°C) @ 40% RH	Water content (%)
25	0.698
45	0.023
T (°C) @ 90% RH	**Water content (%)**
25	2.341
45	1.704

Table B-4: Measurements on 5 cm × 5 cm × 5 mm CZ using TPS- humidifier assembly (TPS 2500S, ThermTest Inc., Fredericton, Canada and Cellkraft F-series humidifier) with power of 10 mW, measurement time of 40 s and rest intervals of 24 hours

RH (%) @ 25°C	k ($W \cdot m^{-1} \cdot K^{-1}$)
0	0.0156
40	0.0164
80	0.0179
RH (%) @ 45°C	**k ($W \cdot m^{-1} \cdot K^{-1}$)**
0	0.0162
40	0.0175
80	0.0186

Table 0-5: Measurements on 30.5 cm × 30.5 cm × 10 mm CZ using HFM @ 25˚C and 7 mm × 7 mm × 10 mm CZ using TMA (Q400EM, TA Instruments) with a macro-expansion probe of a 6.07 mm diameter and @ 25˚C

Stress (kPa) HFM	Strain (%)
0.69	0.00
1.38	5.27
2.34	8.55
3.44	11.17
4.48	13.36
6.55	17.17
7.58	19.53
7.92	20.18
Stress (kPa) TMA	**Strain (%)**
0.37	0.00
1.81	9.37
3.27	14.07
4.72	17.15
6.18	19.46
7.63	21.32

Table 0-6: Measurements on 30.5 cm × 30.5 cm × 5 mm CZ using HFM @ 25˚C and 7 mm × 7 mm × 5 mm CZ using TMA (Q400EM, TA Instruments) with a macro-expansion probe of a 6.07 mm diameter and @ 25˚C

Stress (kPa) HFM	Strain (%)
0.69	0.00
1.38	3.44
2.34	7.083
3.45	9.77
4.48	11.86
Stress (kPa) TMA	**Strain (%)**
0.37	0.00
1.13	9.37
1.89	14.07
2.64	17.15
3.40	19.46
4.15	21.32

ThermalWrap

Table 0-7: Measurements on 30.5 cm × 30.5 cm × 10 mm TW using HFM (Netzsch HFM 436 Lambda) @ RH=0%, compressive load=0.5 Psi and temperature gradient= 40˚C following ASTM C518

T (°C)	k ($W \cdot m^{-1} \cdot K^{-1}$)
-20	0.019
-10	0.020
0	0.020
10	0.021
20	0.022
30	0.022
40	0.023
50	0.024
60	0.025
70	0.026
80	0.027

Table 0-8: Measurements on 30.5 cm × 30.5 cm × 10 mm TW using environmental chamber, ESPEC Platinous series EPX-4H and Ohaus Adventurer™ Balance following ISO 12571:2013 Standard

T (°C) @ 40% RH	Water content (%)
25	1.240
45	0.854
T (°C) @ 90% RH	**Water content (%)**
25	2.870
45	1.157

Table 0-9: Measurements on 5 cm × 5 cm × 5 mm TW using TPS- humidifier assembly (TPS 2500S, ThermTest Inc., Fredericton, Canada and Cellkraft F-series humidifier) with power of 10 mW, measurement time of 40 s and rest intervals of 24 hours

RH (%) @ 25°C	k ($W \cdot m^{-1} \cdot K^{-1}$)
0	0.0215
40	0.0228
80	0.0238
RH (%) @ 45°C	**k ($W \cdot m^{-1} \cdot K^{-1}$)**
0	0.0225
40	0.0240
80	0.0252

Table 0-10: Measurements on 30.5 cm × 30.5 cm × 8 mm TW using HFM @ 25˚C and 7 mm × 7 mm × 8 mm TW using TMA (Q400EM, TA Instruments) with a macro-expansion probe of a 6.07 mm diameter and @ 25˚C

Stress (kPa) HFM	Strain (%)
0.69	0.00
1.38	5.09
2.41	8.75
3.44	11.23
4.48	13.42
5.51	15.25
6.54	16.84
Stress (kPa) TMA	**Strain (%)**
0.37	0.00
1.54	0.09
2.70	0.15
3.86	0.19
5.03	0.23
6.19	0.25

Table 0-11: Measurements on 30.5 cm × 30.5 cm × 5 mm TW using HFM @ 25˚C and 7 mm × 7 mm × 5 mm TW using TMA (Q400EM, TA Instruments) with a macro-expansion probe of a 6.07 mm diameter and @ 25˚C

Stress (kPa) HFM	Strain (%)
0.69	0.00
1.38	4.96
2.41	8.55
3.45	12.40
4.48	14.51
Stress (kPa) TMA	**Strain (%)**
0.35	0.00
1.21	3.50
2.08	6.66
2.95	9.06
3.82	10.98

Appendix C.

Uncertainty Analysis

Thermal conductivity/resistance and mechanical deformation of the aerogel blanket samples were measured three times and the average of the measurements was reported as the final value, the standard deviation of the reported average is obtained from

$$q = \sqrt{\frac{\sum_{i=1}^{n} (q_i - q_{ave})^2}{n}}$$

where n is the total number of measurements, q is the value of measurements and $q_{ave} = \frac{\sum_{i=1}^{n} q_i}{n}$.